



Space Shuttle in NASA Langley  
Helium Tunnel at  $M = 20$   
(NASA SP-440)

## 11. Hypersonic Aerodynamics

### 11.1 Introduction

Hypersonic vehicles are commonplace. There are many more of them than the supersonic aircraft discussed in the last chapter. Applications include missiles, launch vehicles and entry bodies. A huge effort has been made developing hypersonic aerodynamics methods and configurations. This began with missiles, including the intercontinental ballistic missile (ICBM) effort of the 1950s, followed by development work for the Mercury, Gemini and Apollo manned space flight programs. The next major effort was devoted to the Space Shuttle. Work on hypersonics for future entry vehicles and landing of vehicles on other planets continues. Finally, there is a perennial effort to develop atmospheric hypersonic vehicles. These efforts have resulted in a massive literature, and we will provide references for further study. In this chapter we limit our discussion to the key things to know from a configuration aerodynamics viewpoint.

Despite the effort to develop hypersonic configurations, there is no exact definition defining the start of the hypersonic flow regime. Possibilities include:

- a) Mach numbers at which supersonic linear theory fails
- b) Where  $\gamma$  is no longer constant, and we must consider temperature effects on fluid properties.
- c) Mach numbers from 3 - 5, where Mach 3 might be required for blunt bodies causing large disturbances to the flow, and Mach 5 might be the starting point for more highly streamlined bodies.

In this section we will provide a brief outline of the key distinguishing concepts. The books by Bertin and Cummings<sup>1</sup> and Anderson<sup>2</sup> provide a starting point for further study.

Essentially there are five key points to be made:

1. In many cases surface pressure can be estimated fairly easily
2. Control and stability issues lead to different shapes
3. Temperature and aerodynamic heating become critically important
4. Blunt shapes are commonplace
5. Engine-airframe integration is critical

Our discussion will conclude with a summary of the flight vehicles that have been studied extensively and sometimes even flown. Our interest is in the lessons learned from these configurations.

The X-15, shown in Figure 11-1, is the only true manned hypersonic airplane flown to date. It was rocket powered, and started flight by being dropped from a B-52, so it was purely a research airplane. The first flight was by Scott Crossfield in June of 1959. The X-15 reached 314,750 feet in July of 1962 piloted by Joe Walker. An improved version reached a Mach number of 6.7 at an altitude of 102,100 feet in October of 1967 with Pete Knight at the controls. The X-15 program flew 199 flights, with the last one being in October of 1968. Milt Thompson's book<sup>3</sup> describes the X-15 program, including the crackling sounds the airframe made as it heated up!



Figure 11-1. The X-15 (NASA photo)

### 11.2 Surface pressure estimation

In many cases surface pressures are relatively easy to estimate at hypersonic speeds. At supersonic speed we have a local relation for two-dimensional flows relating surface slope and pressure, where  $\theta$  is the surface inclination relative to the freestream:

$$C_p = \frac{2\theta}{\sqrt{M^2 - 1}} \quad (11-1)$$

However, this relation is not particularly useful for most cases in actual aircraft configurations. In comparison, hypersonic rules *are* useful. The most famous relation is based on the concepts of Newton. Although Newton was wrong for low-speed flow, his idea does apply at hypersonic speeds. The idea is that the oncoming flow can be thought of as a stream of particles, that lose all their momentum normal to a surface when they “hit” the surface. This leads to the relation:

$$C_p = 2 \sin^2 \theta \quad (11-2)$$

where  $\theta$  is the angle between the flow vector and the surface. Thus you only need to know the geometry of the body locally to estimate the local surface pressure. Also, particles impact only the portion of the body facing the flow, as shown in Figure 11-2. The rest of the body is in a “shadow”, and the  $C_p$  is assumed to be zero.\* See Bertin and Cummings<sup>1</sup> or Anderson<sup>2</sup> for the derivation of this and other pressure-slope rules.

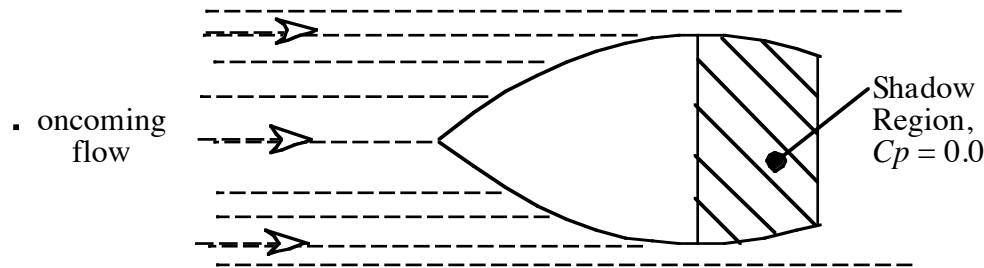


Figure 11-2. Shadow sketch, showing region where  $C_p$  is zero

Two key observations come from the Newtonian pressure rule. First, the Mach number does not appear! Second, the pressure is related to the square of the inclination angle and not linearly as it is in the supersonic formula. This illustrates how the situation in hypersonic flow is significantly different than the linear flow models at lower speeds.

The Newtonian flow model can be refined to improve agreement with data. This form is known as the Modified Newtonian flow formula,

$$C_p = C_{p_{\max}} \sin^2 \theta \quad (11-3)$$

where the stagnation  $C_{p_{\max}}$  is a function of Mach and  $\gamma$ ,

$$C_{p_{\max}} = \frac{P_{02} - P_{\infty}}{\frac{1}{2} \rho_{\infty} V_{\infty}^2} \quad (11-4)$$

and  $P_{02}$  is the stagnation or total pressure behind a normal shock. This expression gets both the Mach number and ratio of specific heats back into the problem. The classical Newtonian theory is actually the limit as  $M \rightarrow \infty$ , and  $\gamma \rightarrow 1$ . These formulas are only valid when  $\theta$  is positive. There are lots of other local rules, and Anderson's book<sup>2</sup> should be consulted for a more complete discussion. These are known as surface inclination rules. The methods normally heard in hypersonic discussions include the tangent cone, tangent wedge and shock expansion methods. There is also a modification to the Newtonian pressure rule to include surface curvature effects. This is known as the Newtonian-Busemann rule.

How well do these methods work? We look at two cases. First we look at a blunt body case, and then we will compare results with the pressure on a circular cone at zero angle of attack.

Figure 11-3 shows the agreement with wind tunnel data for a blunted cone.<sup>4</sup> In this case the agreement is remarkably good for a Mach number of 1.9. Note also that for many hypersonic cases we plot with a different axis direction than classic sub- super-sonic aerodynamics (Note the

\* Recall  $C_{p_{\text{vac}}} = -2/(\gamma M^2)$ , and quickly approaches zero as the Mach number increases.

change in slope at about  $s/r$  of 0.9. The geometry is not a pure hemisphere cone, but has a transition arc). If we had used the pure Newtonian formula the pressure at the nose would have been 2.0. Clearly the modified formula does an excellent job.

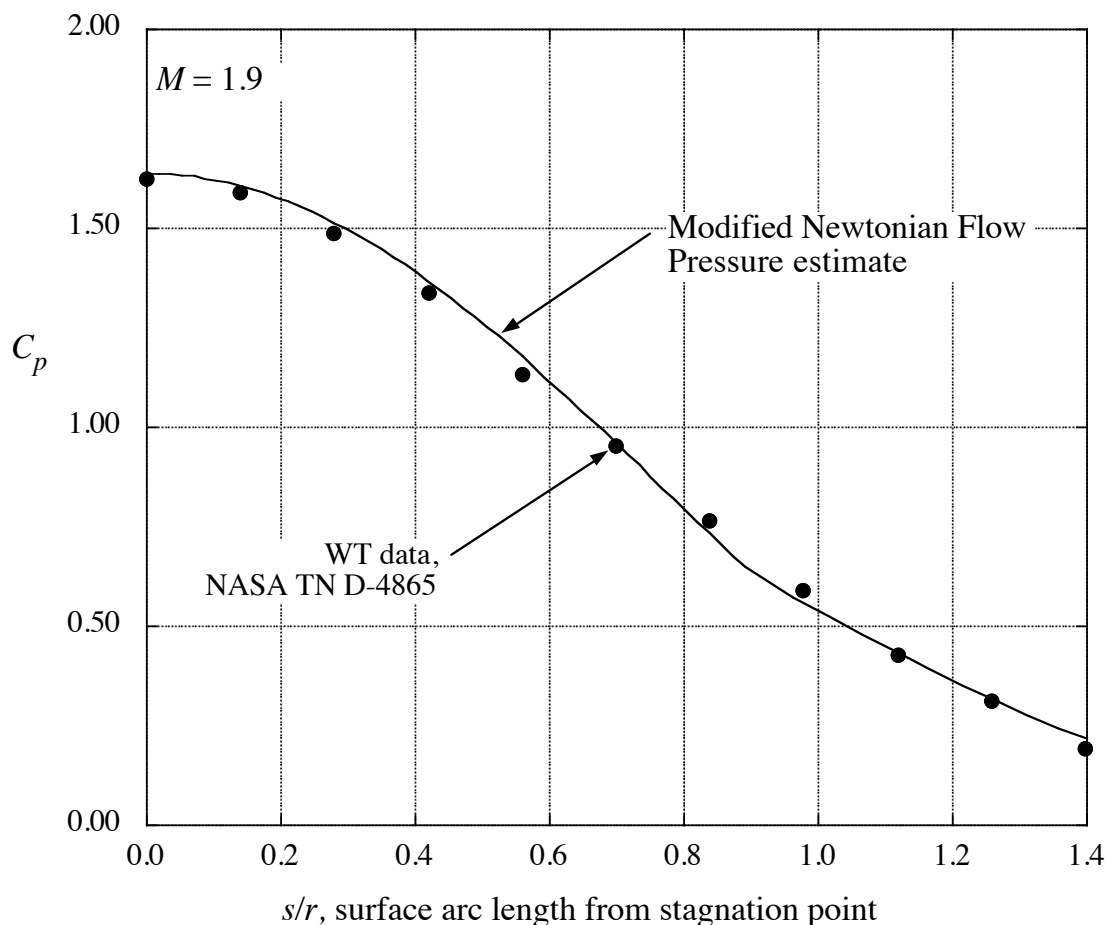


Figure 11-3. Comparison of the modified Newtonian estimate over the nose of a blunted cone with wind tunnel data (Model 2 in TN D-4865).<sup>4</sup>

Next we will examine the results of Newtonian and Modified Newtonian theory together with predictions from a theory given by DeJarnette, et al<sup>5</sup> and the exact results from the NASA Cone Tables.<sup>6</sup> Figure 11-4 shows the surface pressure results over a Mach number range from 4 to 10, and cone angles of 15 and 25 degrees. The cone table results can be considered to be the exact inviscid values. Recall that the cone produces a conical flowfield, and the surface pressure variation is constant along the surface for an attached shock. In this case the Newtonian approximations are not nearly as good.

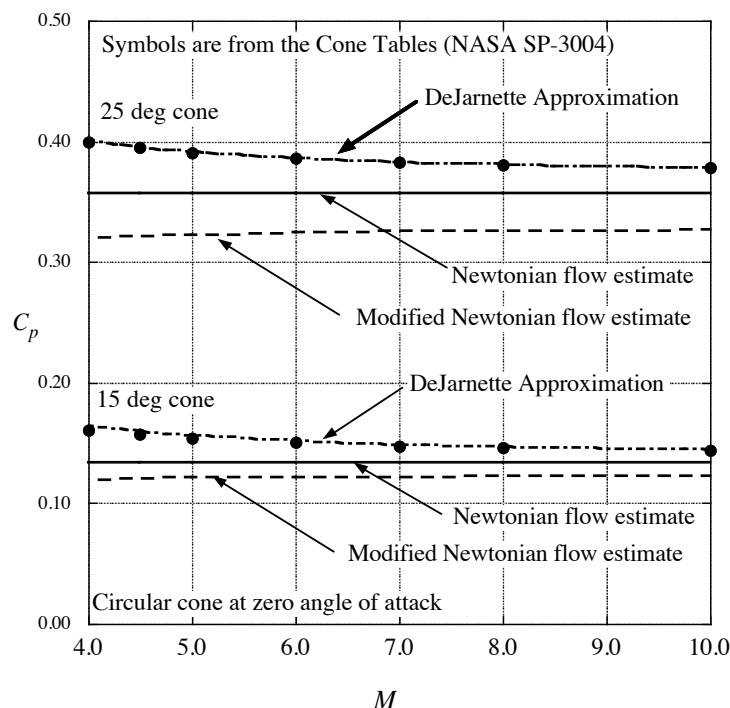


Figure 11-4. Comparison of surface pressures for a cone at zero angle of attack.

Since the Newtonian estimates are not particularly good, we will provide the simple formula from DeJarnette<sup>5</sup> et al that we've shown works well:

$$C_{p_{c=0}} = \sin^2 \delta_c \left[ 1 + \frac{(\gamma+1)K^2+2}{(\gamma-1)K^2+2} \ln \left( \frac{\gamma+1}{2} + \frac{1}{K^2} \right) \right] \quad (11-5)$$

where:

$$K^2 = (M^2 - 1) \sin^2 \delta_c$$

The advantage of the so-called surface inclination rules is that they only need the local geometry. These methods were combined into a program know as the Hypersonic Arbitrary Body Program (HABP) originally developed at Douglas Aircraft and also known as the "Gentry Code." The program is available for free download from the Carmichael's Public Domain Aeronautical Software site.<sup>7</sup> Unfortunately, the user has to be wise enough to choose which rule should be used over various parts of the body.

Once you proceed beyond the early stages of configuration design it is appropriate to use CFD.

While we are looking at surface pressures we should look at the change in physics from subsonic to hypersonic flow. This will be a key concept in configuration development. What is the maximum (fictitious) lift on a flat plate? I call this the "ultimate" lift. The resulting value is given in Figure 11-5. Here the lower surface pressure is taken equal to the stagnation value and the upper surface pressure is taken equal to the vacuum value. We can see that at low speeds the lift is generated on the upper surface, while at high speed the lift is almost completely generated on the lower surface. This will be important when designing hypersonic vehicles.

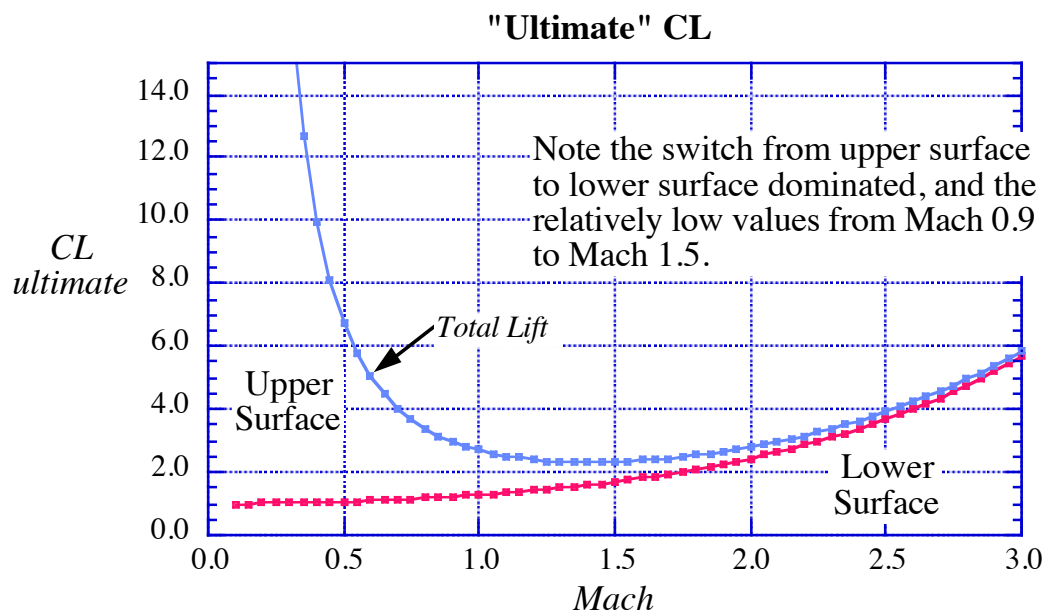


Figure 11-5. The “Ultimate CL” plot (showing the dominance of the lower surface at hypersonic speeds)

### 11.3 Aerodynamic stability and control

For stability, many hypersonic vehicles display an unusual geometric feature. It turns out that thick bases are often used on hypersonic vehicles, and in this section we illustrate why they are desirable. Our example relates to the thick trailing edge on the vertical tail of the X-15, as shown above in Figure 11-1.

The example of the difference in the flow characteristics at hypersonic speed will be used in the *hypersonic directional stability problem*. To start, we consider the yawing moment contribution from the vertical tail, which is

$$N_{VT} = q_{VT} S_{VT} l_{VT} C_{Y_{VT}} \quad (11-6)$$

where  $q_{VT}$  is the dynamic pressure at the vertical tail,  $S_{VT}$  is the vertical tail area,  $l_{VT}$  is the moment arm and  $C_{Y_{VT}}$  is the side force coefficient. The standard definition of  $C_n$  is:

$$C_n = \frac{N}{q_{ref} S_{ref} b_{ref}} \quad (11-7)$$

We can write the yawing moment due to the vertical tail as:

$$C_{n_{VT}} = \underbrace{\frac{l_{VT} S_{VT}}{b_{ref} S_{ref}}}_{\substack{\text{vertical tail} \\ \text{volume} \\ \text{coefficient, } V_{VT}}} \cdot \underbrace{\frac{q_{VT}}{q_{ref}}}_{\substack{\text{ratio of} \\ \text{dynamic pressures} \\ \text{assume } \approx 1}} \cdot C_{Y_{VT}} \quad (11-8)$$

The nomenclature associated with the problem and the equations is illustrated in Figure 11-6.

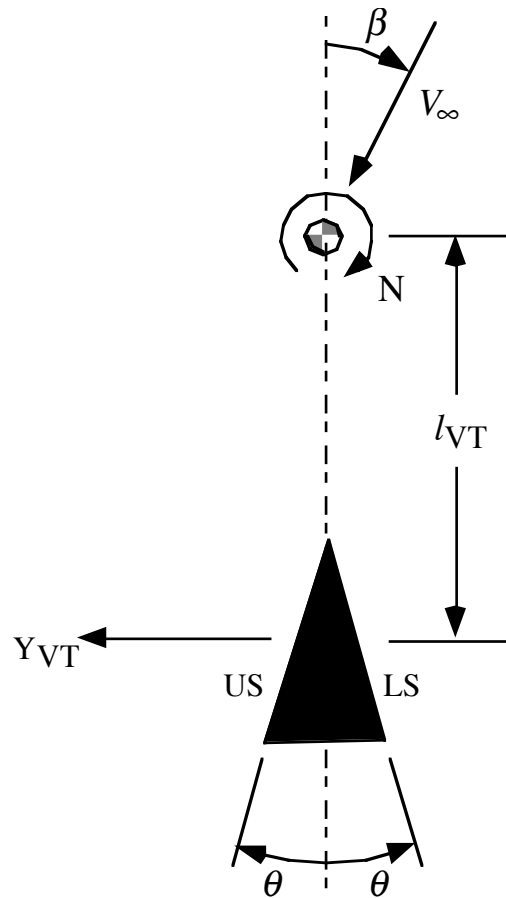


Figure 11-6. Sketch defining the hypersonic directional stability problem

Now, for a high-speed flow, we will assume that the vertical tail is a two-dimensional surface with a constant pressure on each side, so that  $C_{Y_{VT}} = C_{P_{LS}} - C_{P_{US}}$ . We will consider two cases, one supersonic, the other hypersonic. We compare the results for directional stability at high Mach number using the two-dimensional rule for linearized supersonic flow and Newtonian theory for hypersonic flow, as shown below.

<u>Linear theory</u>	<u>Newtonian theory</u>	
$C_p = \frac{2\theta}{\sqrt{M^2 - 1}}$	$C_p = 2\sin^2\theta$	(11-9)

Case 1: Linearized supersonic theory

$$C_{Y_{VT}} = \Delta C_p = \frac{2(\theta + \beta)}{\sqrt{M^2 - 1}} - \frac{2(\theta - \beta)}{\sqrt{M^2 - 1}} = \frac{4\beta}{\sqrt{M^2 - 1}} \quad (11-10)$$

showing that the  $\theta$ 's cancel. We use this expression to get  $C_{n_\beta}$ :

$$C_{n_{\beta_{VT}}} = V_{VT} \frac{\partial C_{Y_{VT}}}{\partial \beta} = V_{VT} \frac{4}{\sqrt{M^2 - 1}} \quad (11-11)$$

This expression shows that  $C_{n\beta}$  is positive, but vanishes for hypersonic Mach numbers.

*Case 2: Hypersonic flow theory, Newtonian theory*

This time the expression for the side force is:

$$C_{Y_{VT}} = \Delta C_p = 2\sin^2(\theta + \beta) - 2\sin^2(\theta - \beta) \quad (11-12)$$

Using trig functions:

$$C_{Y_{\beta VT}} = 2 \left[ \begin{array}{l} \sin^2 \theta \cos^2 \beta + 2 \cos \theta \sin \beta \sin \theta \cos \beta + \cos^2 \theta \sin^2 \beta \\ -\sin^2 \theta \cos^2 \beta + 2 \cos \theta \sin \beta \sin \theta \cos \beta - \cos^2 \theta \sin^2 \beta \end{array} \right] \quad (11-13)$$

This reduces to:

$$\begin{aligned} C_{Y_{\beta VT}} &= \underbrace{8}_{=1} \underbrace{\cos \theta}_{=\beta} \underbrace{\sin \beta}_{=\theta} \underbrace{\sin \theta}_{=1} \cos \beta \\ &\equiv 8\theta\beta \end{aligned} \quad (11-14)$$

and at  $\beta = 0$ :

$$C_{n_{\beta VT}} = 8V_{VT}\theta \quad (11-15)$$

If  $\theta$  is zero, so is  $C_{n\beta}$ ! But opening up the angle rapidly increases  $C_{n\beta}$ . In addition, there is no Mach number dependence. The Case 2 results were verified experimentally, and the wedge vertical tail concept literally saved the X-15 program.<sup>8</sup> This effect is also the reason for flared “skirts” seen on some launch vehicles. Figure 11-7 shows the airplane at the Smithsonian Air and Space Museum on the Mall in Washington DC. This is a photo I took to highlight the wedge vertical tail with the large base area. This “airfoil” results in significant base pressure drag. However, the airplane was rocket propelled and had enough thrust so that the base drag wasn’t critical.

This analysis brings out another key issue. For a flat plate at hypersonic speeds the use of the classic stability derivative concept is problematic.  $C_{L\alpha}$  is no longer a constant with angle of attack. This means that the stability and control analysis has to be generalized.

There is, however, more to the story. Lets take another look at the X-15.



Figure 11-7. X-15 on display at the National Air and Space Museum.

Now let's look at the top and side view of the airplane in Figure 11-8.<sup>9</sup> The wedge vertical tail can be seen again in the top view. However, we are really interested in the side view. Note the ventral fin portion of the vertical tail. The lower dashed portion of the ventral tail was designed to be dropped before landing. This turned out to be a fortuitous design feature.

To reenter the atmosphere a “hi- $\alpha$ ” recovery was desired. Initial lateral-directional data for the simulator was for the horizontal stabilizer at zero deflection. Once the math model was updated, above 15 degrees angle of attack there was a PIO (Pilot Induced Oscillation) if the SAS (Stability Augmentation System) was inoperative. After the aero characteristics were updated the roll damper was flight critical. Loss of the SAS above 200,000 ft altitude would result in loss of the aircraft. It turns out that although  $C_{n\beta}$  was good, the  $C_{l\beta}$  was poor. Bob Hoey,<sup>10</sup> who was one of the flight test engineers, described this story. The problem was the adverse rolling moment created by the large ventral fin. Although the airplane had plenty of directional stability, the dihedral effect was strongly negative at high alpha (left sideslip produced left roll). Famous flight test pilot Joe Walker said it was “like a marble rolling on the outside of a barrel.”

The fix proposed by the flight test engineers was to simply leave the detachable portion of the ventral fin off.  $C_{n\beta}$  was reduced but  $C_{l\beta}$  was now acceptable at high alpha and Dutch roll was

“about the same.” This was counterintuitive since vertical tail size was typically being increased after flight testing at that time (recall the F-100 story in Chapter 9).

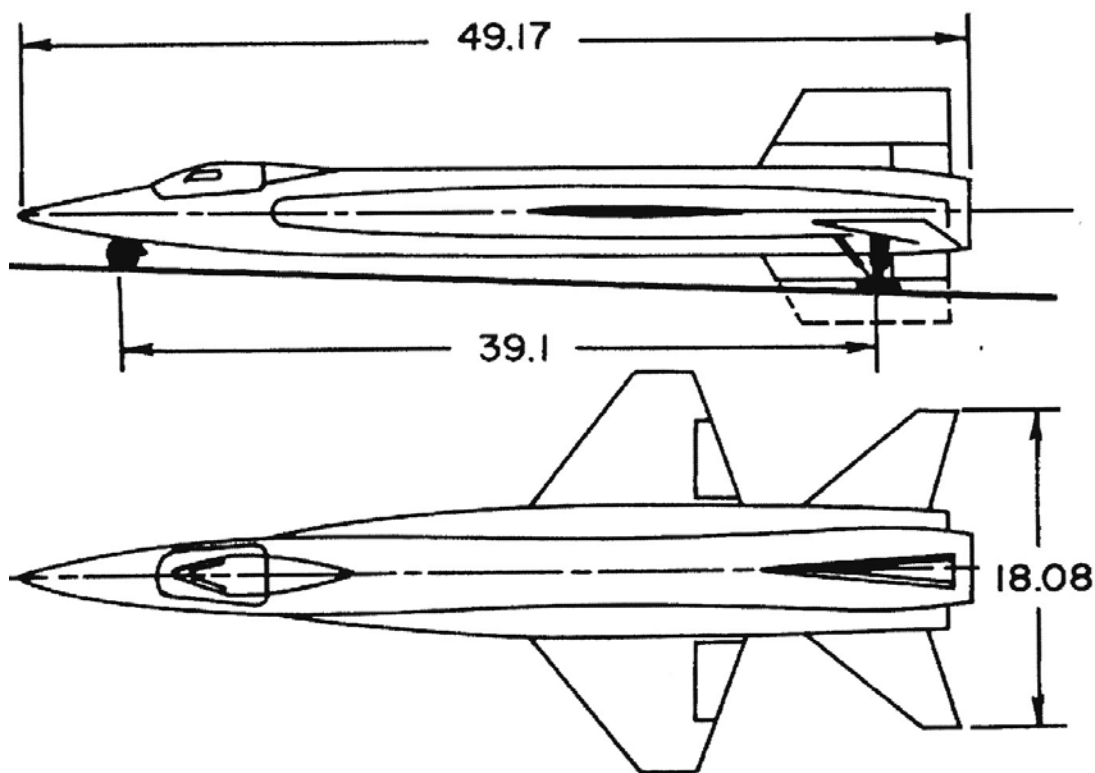


Figure 11-8. Side and top view drawings of the X-15. Note the dashed lines outlining a portion of the ventral tail.<sup>9</sup>

It is worthwhile to look at the stability derivatives as presented by Roxanah Yancy.<sup>9</sup> Figure 11-9 contains the directional data and Figure 11-10 presents the lateral data.

Specifically, look at the  $\alpha = 15^\circ$  to  $25^\circ$  portion of Figures 11-9 and 11-10. Leaving the lower portion of the ventral off reduces  $C_{n\beta}$  compared to keeping it on. At a Mach number below 3  $C_{n\beta}$  goes negative. However at this speed the angle of attack can be reduced and  $C_{n\beta}$  becomes positive. In exchange for sacrificing strongly positive  $C_{n\beta}$  (directional stability), Figure 11-10 shows that  $C_{l\beta}$  is now at least slightly negative. The pilots found this acceptable. These figures should be studied very carefully. This is an important example of configuration aerodynamics understanding and thinking to achieve a viable configuration.

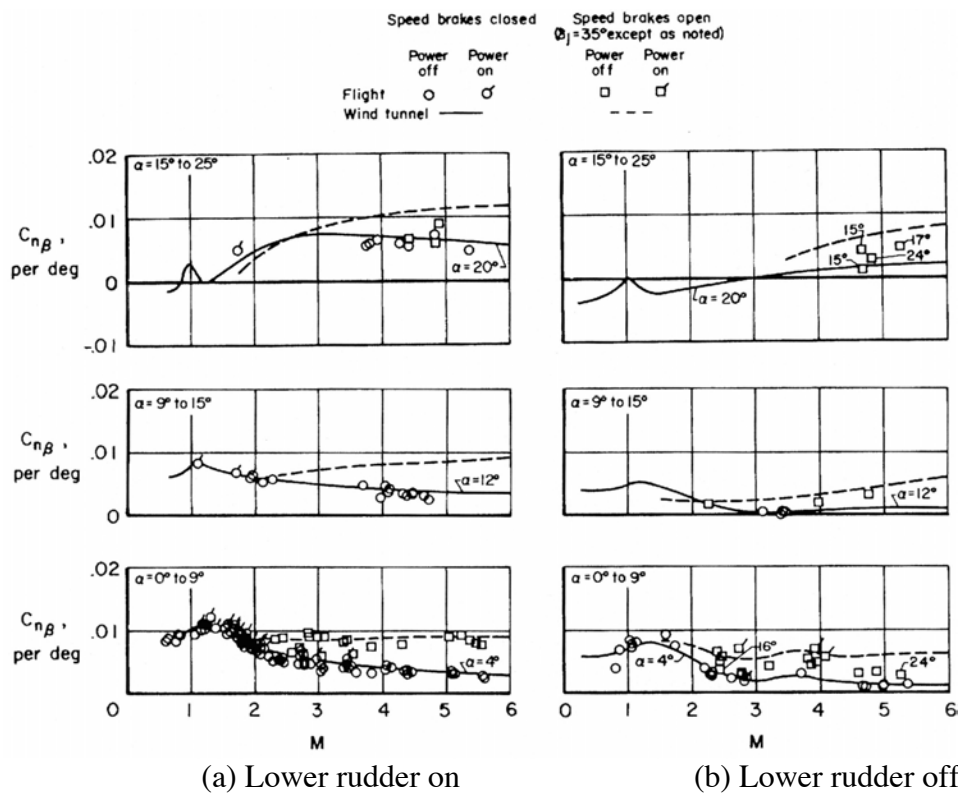


Figure 11-9 Directional data (NASA TN D-2532<sup>9</sup>)

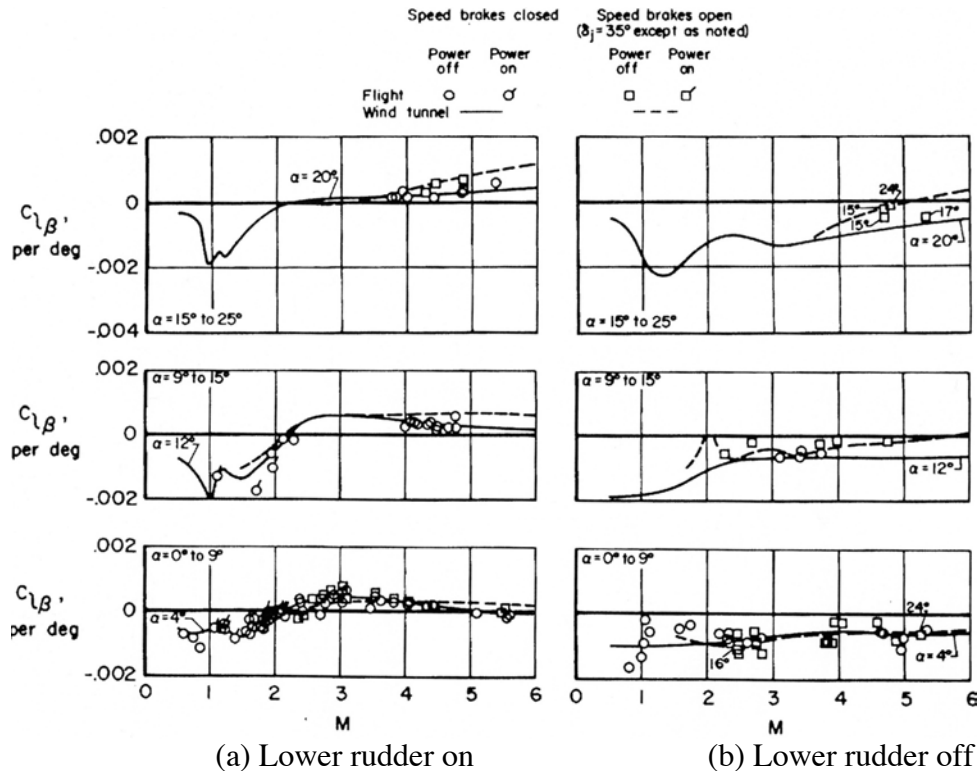


Figure 11-10 Lateral data. (NASA TN D-2532<sup>9</sup>)

### 11.4 Aerodynamic Heating

We are now ready to address what is probably the most challenging consideration in developing hypersonic vehicles. This is illustrated by looking at the relationship between stagnation temperature and static temperature:

$$\frac{T_0}{T} = 1 + \frac{\gamma - 1}{2} M_\infty^2 \quad (11-16)$$

Or the adiabatic wall temperature

$$T_{adiabatic\ wall} = \left( 1 + r \frac{\gamma - 1}{2} M_\infty^2 \right) T_e \quad (11-17)$$

where  $r$  is the recovery factor. As noted, Eq. 11-17 is for an adiabatic (no heat transfer) wall temperature. For many hypersonic vehicles the surface will have to be cooled and the heating needs to be estimated. For adiabatic wall temperatures the limit for an aluminum structure is around Mach 2, which was the Concorde's cruise Mach number. The SR-71 was made of titanium and temperature limited the speed to slightly over Mach 3. Note that some sources indicate that this limit was actually the temperature limit on the wiring inside the airplane, and that is the condition that limited the speed.

Thus hypersonic aerodynamic configuration design means that you must always deal with heating. In general, at sustained high speeds surfaces must be cooled, and since heating is a critical concern, this means that viscous effects are crucial immediately. Also, unlike normal airplane aerodynamics, hypersonic vehicles fly at very high altitudes and the Reynolds number may be low enough that the flow is laminar. This means laminar flows are also often of interest. Recall that the heat transfer is much lower when the flow is laminar. In fact, being able to estimate the transition location (for these cases transition occurs over a region, and can't be assumed to occur at a "location") with certainty is a critical requirement in hypersonic vehicle design, and is the subject of current research.<sup>11</sup> A description of the aerodynamic heating on the SR-71 is available in the excellent paper by Ben Rich.<sup>12</sup> An appendix in his paper provides the equations used to estimate the heat transfer coefficients.

In the 1950s the problem of aerodynamic heating was a problem of national focus. The ability of ICBMs to reenter the atmosphere and accurately deliver the payload was a critical requirement. Initially it had been assumed that the nose shape should consist of a sharply pointed tip. However, H. Julian Allen and A.J. Eggers at NACA Ames found that a blunt shape would be much better. A blunt nose forces a detached shock wave and most of the heat goes off the surface and into the flowfield, not the vehicle. This insight enabled practical reentry "vehicles." Thus, a nose or leading edge radius large enough to prevent the nose from melting had to be used. The analysis by H. Julian Allen and A.J. Eggers convinced the aerodynamic design community that blunt bodies were required to survive entry from orbit.<sup>13</sup>

The maximum value of the heat transfer,  $q\text{-dot}$ , is proportional to the leading edge radius as shown in this relation:

$$\dot{q}_{\max\ laminar} = \frac{1}{\sqrt{R_{LE}}} \quad (11-18)$$

where  $R_{LE}$  is the leading edge radius at the stagnation point. Clearly, a larger  $R_{LE}$  is desirable.

This result led to the choice of the manned space capsule shapes for the Mercury, Gemini and Apollo programs. The Space Shuttle entered the atmosphere at a very high angle of attack so that it was in effect a blunt body. Figure 11-11 show a photo of Harvey Allen demonstrating the concept.

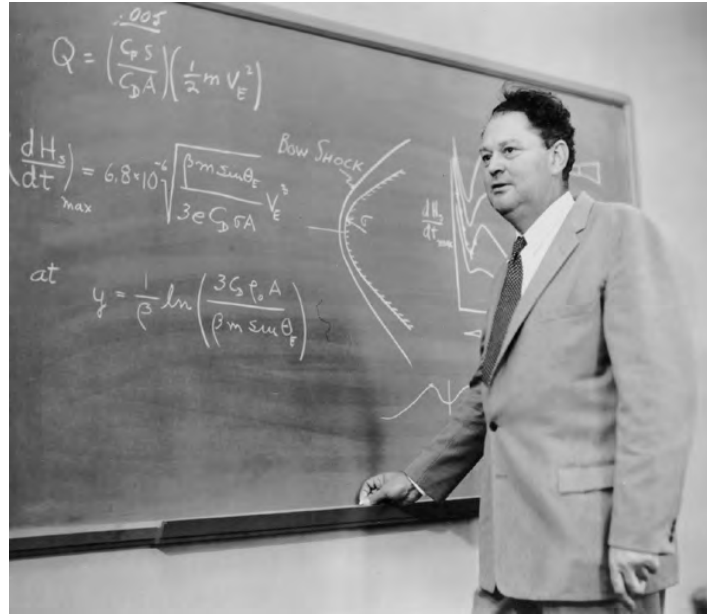


Figure 11-11. Harvey Allen at NASA Ames. (NASA Photo)

Figure 11-12 shows an example of the flowfield over a sphere at a Mach number of 7.6. The so-called shock standoff distance was critically important and its estimation was one of the important efforts at the time.

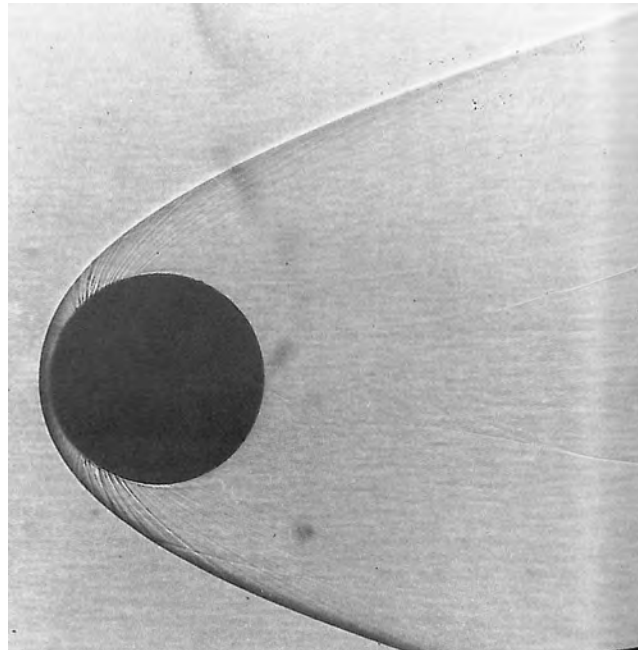


Figure 11-12. Photo of  $M = 7.6$  flow over a sphere (from Van Dyke, *An Album of Fluid Motion*,<sup>14</sup> originally from the Naval Surface Weapons Center).

Even when using a blunt body re-entry shape the heating problem is severe. The Mercury, Gemini and Apollo vehicles used an ablative heat shield, where portions of the shield actually burn off. The Space Shuttle, which re-entered from a relatively low earth orbit, used special heat resistant tiles, a number of which had to be replaced after each flight. Details of the Apollo capsule thermal protection system can be found in the reference by Pavlosky and Leger.<sup>15</sup>

This was the first great challenge problem for CFD (this was in the 1960s, and the computational solution of the flowfield wasn't called CFD until the early 1970s). It is known as "the Blunt Body problem". It was particularly difficult because the flow is subsonic behind the strong normal, or nearly normal, shock wave. The flow then accelerates quickly to supersonic/hypersonic speed. Thus this is the reverse of the transonic flow problem. Now the freestream is supersonic/hypersonic rather than subsonic. We want to know the shock standoff distance, the shock shape, and the flow properties at the nose, where the aerodynamic heating is highest. The shape of the shock determines the distribution of flow properties such as entropy, which vary as the shock slope changes.

The problem was solved by computing the unsteady flowfield, which is always mathematically hyperbolic. If the solution is steady, the computation will converge to the steady state result while overcoming the difficulty of the mixed elliptic-hyperbolic equation type that describes the steady state problem. The successful approach invented to obtain a practical blunt body calculation method is generally attributed to Moretti.<sup>16</sup>

In case the issue of aerodynamic heating seems academic, consider the  $M = 6.7$  flight of the X-15. It turned out to be the last flight of that airplane. A dummy scramjet\* installation was tested by placing the scramjet mockup below the airplane. The shocks from the front of the scramjet inlet impinged on the pylon supporting the scramjet. The shock interference heating was so severe that the shocks acted as a blowtorch, cutting through the structure, and effectively slicing off the scramjet. The internal damage to the airplane from the heating led to the scrapping of this high-speed version of the airplane, and terminated the program. Figure 11-13 below shows the scramjet hanging below the airplane.

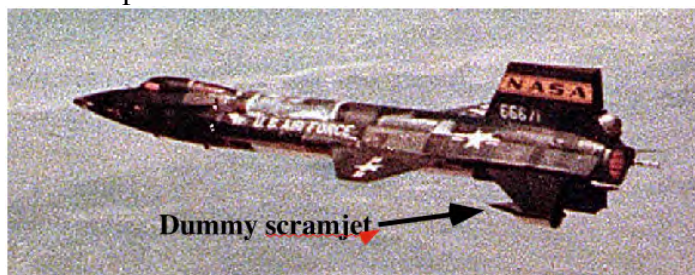
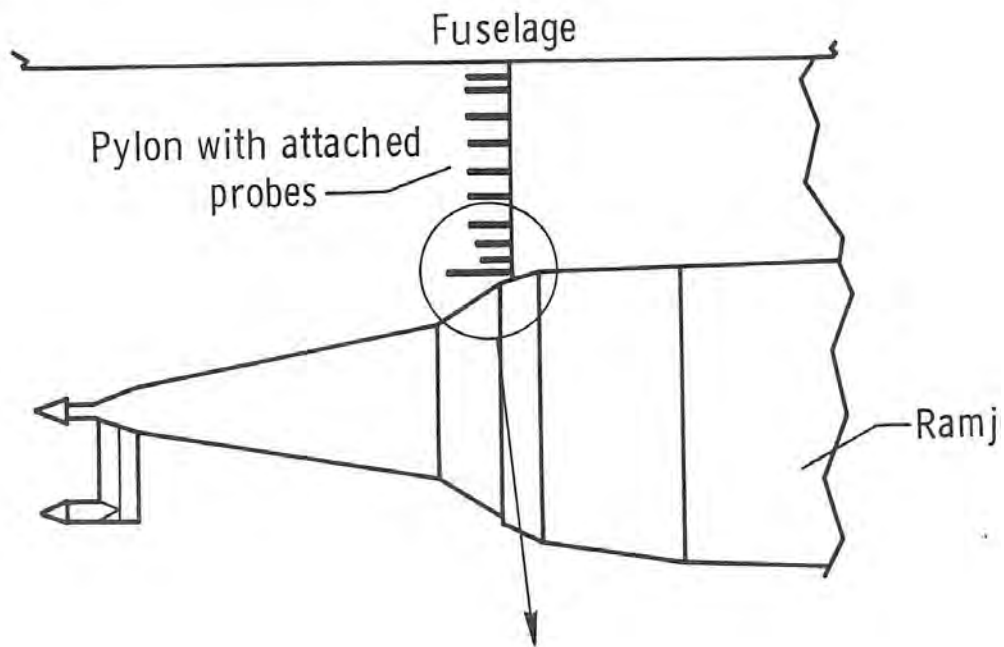


Figure 11-13. X-15 with dummy scramjet (Picture from the NASA Dryden Photo Web Site)

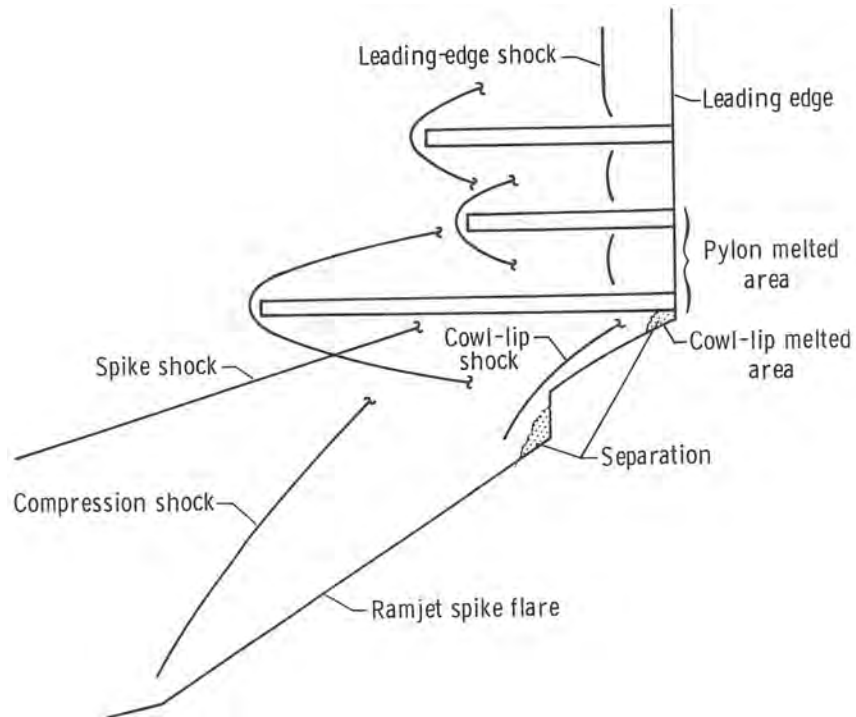
Figure 11-14 shows a schematic representation of the scramjet installation. Apparently this was done in an ad hoc fashion without serious analysis. Figure 11-15 shows the result. This was an indication of the seriousness of the aerodynamic heating problem. Both of these figures are contained in the paper by Iliff and Shafer,<sup>17</sup> taken directly from NASA TM X-1669.<sup>18</sup>

---

\* A scramjet is similar to a ramjet, but the flow through the combustion chamber is supersonic. This has been a difficult technology to develop, but has been demonstrated in flight, see the discussion later in this chapter.



(a) overview of scramjet installation



(b) illustration of assumed shock patterns

Figure 11-14. Schematic of the scramjet installation. (Iloff and Shafer,<sup>17</sup> and NASA TM X-1669<sup>18</sup>)

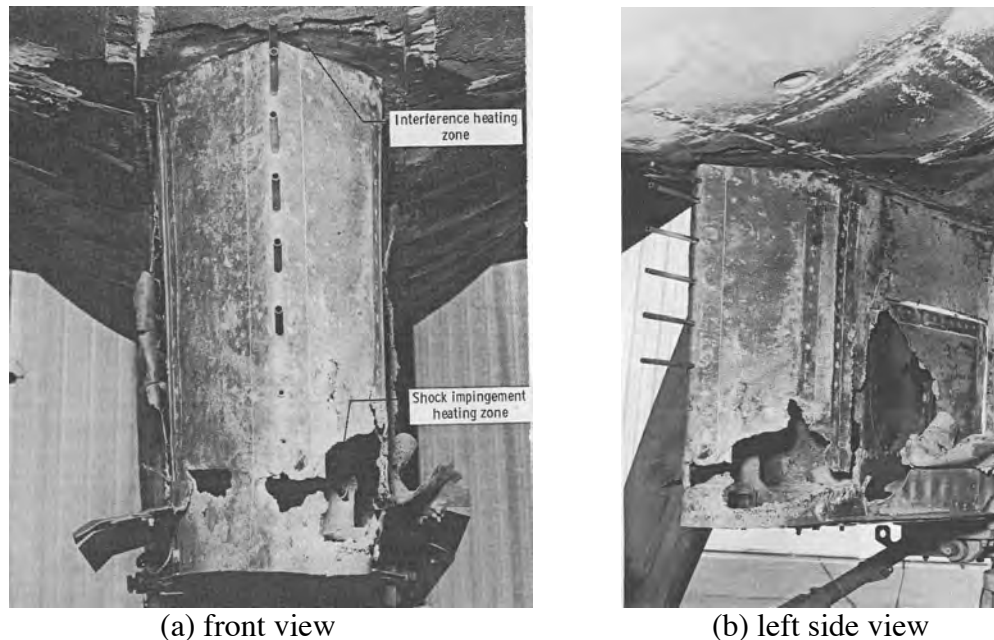


Figure 11-15. The result of aerodynamic heating at  $M = 6.7$  (NASA TM X-1669<sup>18</sup>)

The message from this “incident,” as it was described, is that shock impingement on a surface at hypersonic speed leads to extreme heating. Special care must be taken when developing a hypersonic configuration to avoid shock impingement heating.

Also, recall that the Space Shuttle Columbia was destroyed by the breakdown of the thermal protection system on Feb. 1, 2003. In that case a piece of insulating foam from the external tank broke off during ascent and damaged the leading edge of the Space Shuttle, exposing the internal structure to the heating during re-entry. There was essentially nothing left to see when debris was found compared to the X-15 case we’ve shown. Some of the recent flight test vehicles have also been lost due to adverse effects of aerodynamic heating.

### 11.5 Additional Gas Dynamics Considerations

Because of the severe conditions many somewhat unique and distinctive gas dynamics effects become important. These effects are the result of a difference in the viscous effects at hypersonic speeds. Specifically, flight at high altitudes leads to a significant extent of laminar flow. Also, Mach number effects (heating in particular) result in a thicker boundary layer. Figure 11-16 from Hayes and Probstein<sup>19</sup> illustrates the situation.

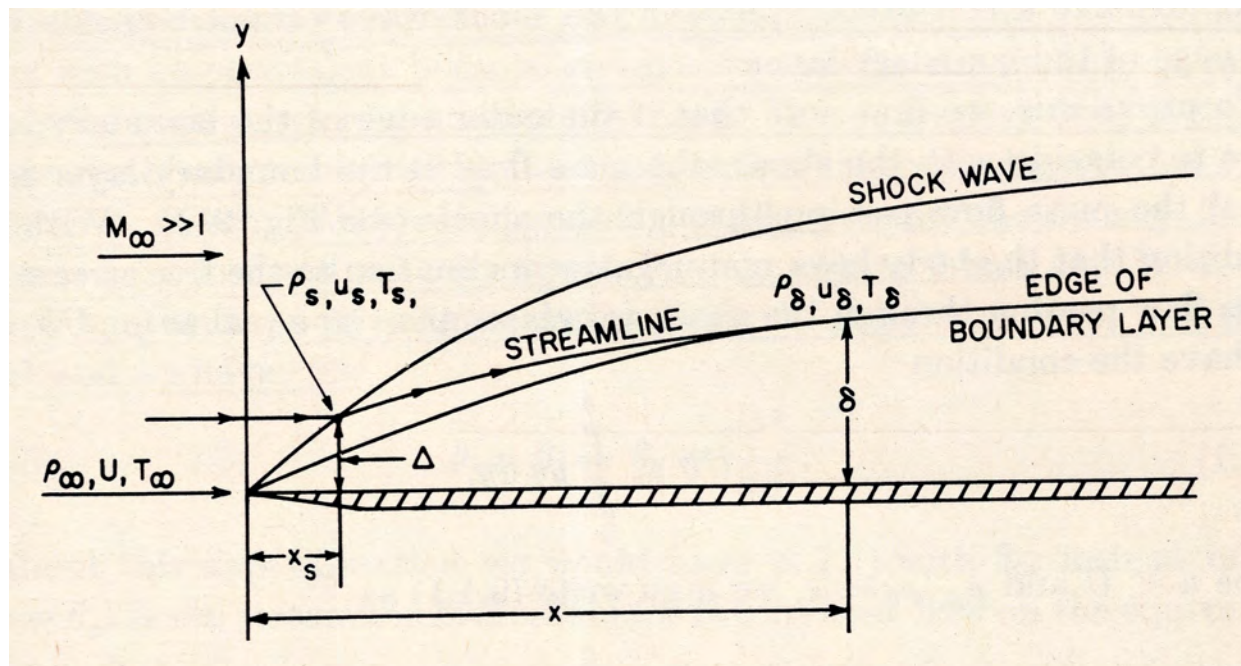


Figure 11-16 Boundary layer development on a flat plate at hypersonic speed.<sup>19</sup>

The thicker hypersonic boundary layer means that it immediately affects the pressure distribution compared to the low speed case where the flow over a “flat plate” surface in line with the freestream flow will not change the pressure distribution significantly. An example of this effect on pressures is shown in Figure 11-17, where pressures were measured on a plate at zero alpha and  $M = 6.86$ .<sup>20</sup> At low speeds we would expect  $p_2 - p_1$  to be zero. Especially near the leading edge there is an effect of the boundary layer on the pressures. This effect is known as viscous-inviscid interaction and can be characterized as either “strong” or “weak.” An extensive description is available in Hayes and Probstein.<sup>19</sup> Once again, modern CFD needs to be used in design, and this flow feature should arise without having to be deeply involved in the theory.

As shown above, viscous compressibility effects can be important. We illustrate this by looking at the skin friction drag coefficient change on a flat plate with increasing Mach number. The code FRICTION can be used to study this effect.<sup>21</sup> As posted on the web site, the code assumes that the wall is at the adiabatic wall temperature (no heat transfer). This is the usual assumption for typical aircraft aerodynamics, say up to a Mach number of 2. However, the hardwired value of the ratio of the wall temperature to the adiabatic wall temperature, TWTAW, can be easily changed. Figures 11-18 and 11-19 show the variation of skin friction drag coefficient for an adiabatic wall and values of the wall temperature to freestream temperature ratios of 0.25, 1.0 and 4.0. The laminar results use the Eckert Reference Temperature Method to incorporate Mach number and wall temperature effects.<sup>22</sup> The turbulent results use the Van Driest II Method.<sup>23</sup> The values are given normalized by the zero Mach number adiabatic wall value. In general the skin friction coefficient decreases with increasing Mach number and wall temperature.

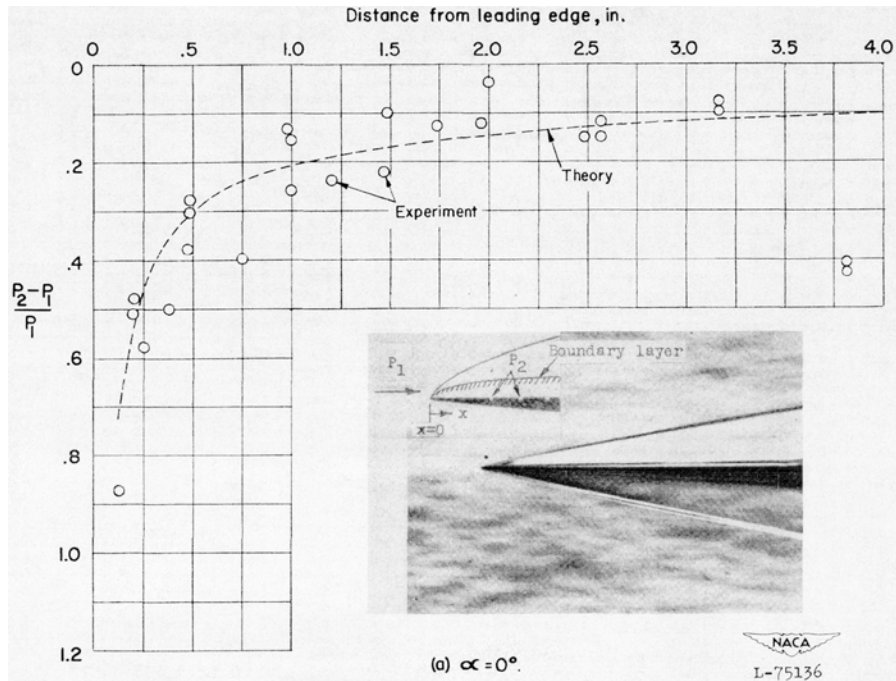


Figure 11-17. Experimental results over a flat plate at zero angle of attack,  $M = 6.86$ ,  $Re = 0.98$  million from Bertram, NACA TN 2773.<sup>20</sup>

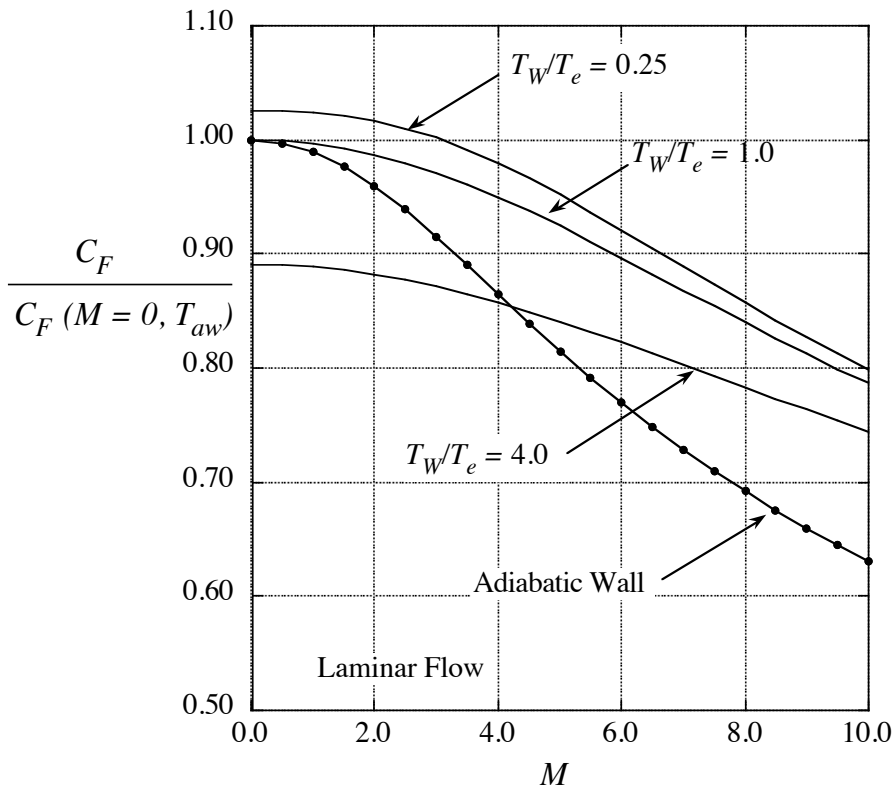


Figure 11-18 Compressibility effects on flat plate skin friction drag coefficient for laminar flow

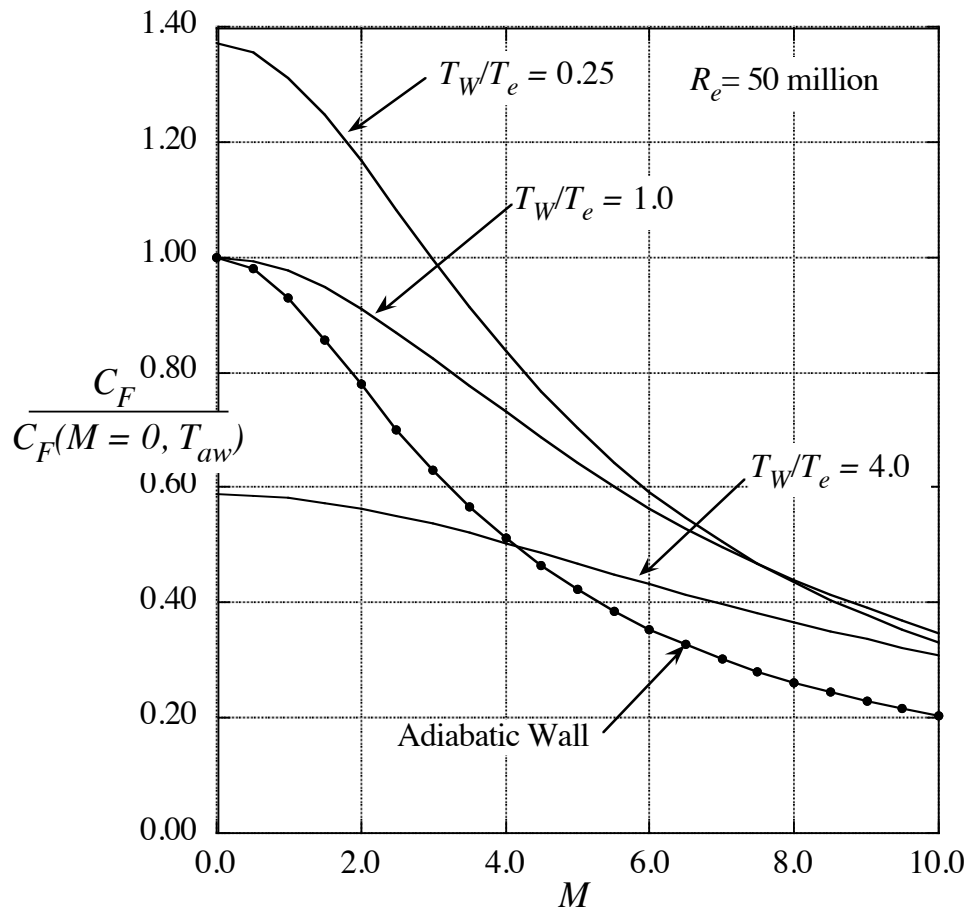


Figure 11-19 Compressibility effects on flat plate skin friction drag coefficient for turbulent flow

At one time theoretical aerodynamicists devoted a large part of their efforts to developing prediction methods for viscous-inviscid interaction methods to predict these effects. Today we can use CFD to find the hypersonic flowfield. The most recent overview of CFD for hypersonic flow appeared in a special issue of the *Journal of Spacecraft and Rockets*.<sup>24</sup> Finally, an excellent chart sent to me by Chris Johnston at NASA Langley illustrates the range of considerations that might be important when making hypersonic aerothermodynamic predictions.<sup>25</sup> Figure 11-20 presents the chart and provides a conclusion for this section.

For a much more thorough description of these effects study the books by Bertin<sup>26</sup> and Hirschel and Weiland.<sup>27</sup> Also, an excellent discussion of aerothermodynamics is available in the survey paper by Hollis and Borrelli.<sup>28</sup> This paper includes a discussion of radiation effects. These also have to be included when the entry velocities become extremely high.

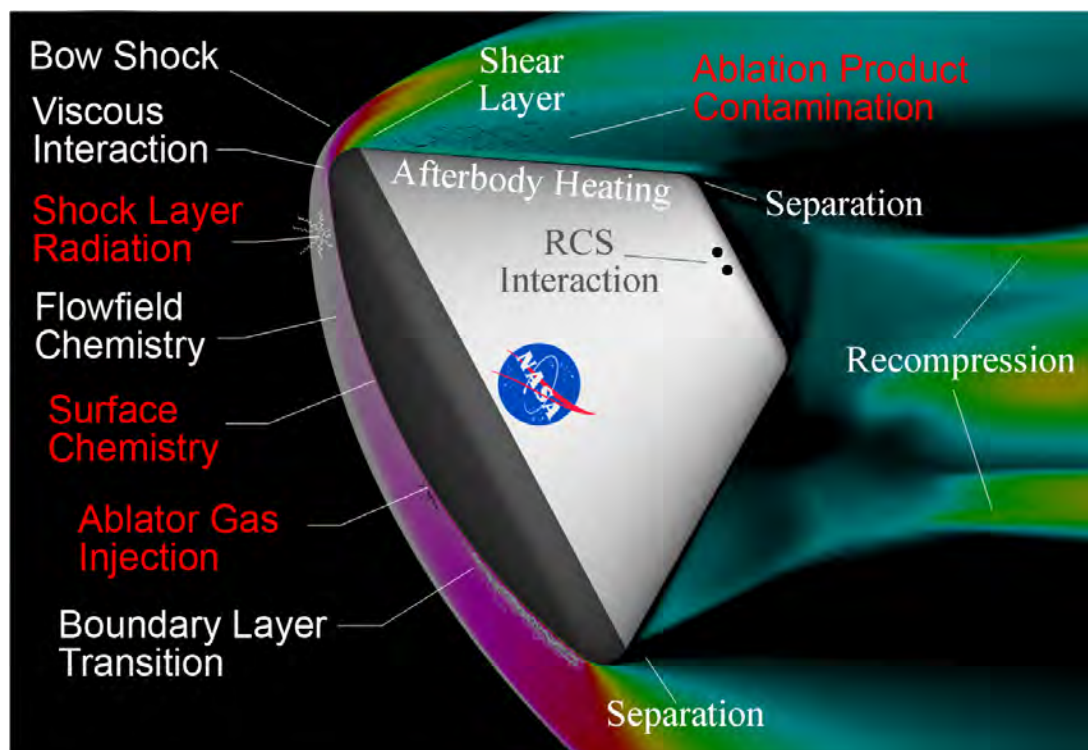


Figure 11-20. The range of gas dynamic consideration required to predict re-entry flowfields.

### 11.6 High Temperature Gas Dynamics Considerations

We now briefly discuss the effects of high temperatures on gas dynamic properties. Coming from the classic subsonic through supersonic aerodynamic viewpoint we almost always assume a calorically and thermally perfect gas. This means that the ratio of specific heats,  $\gamma$ , is a constant. At high temperatures this is no longer the case. Anderson<sup>2</sup> makes the point that this effect should be called “high temperature gas dynamics.” It is very common in the community and in the literature to describe this as a “real gas” effect, which is not precisely correct. In addition, the gas can be in equilibrium or “reacting” in time and space. If the flow composition is varying in time additional equations must be added to the governing equation set. This situation is known as including finite rate chemistry. Here we will present the difference between our classical constant gamma gas dynamics and air that is in equilibrium. The values plotted are from tables generated at the Cornell Aeronautical Lab.<sup>29</sup> An engineering applet is available to compute the same information.<sup>30</sup> The applet uses the so-called “Tannehill Curve Fits”.<sup>31</sup> Figure 11-21 shows the difference between calorically perfect gas and equilibrium values for the temperature behind a normal shock wave. In this case we present results for two different altitudes as a function of freestream Mach number. The equilibrium air results also depend on the freestream value of pressure. Note that the Mach number is not necessarily an appropriate reference value for equilibrium and finite-rate chemistry flows, and you will not necessarily see results presented in this fashion. However, from a “low speed” perspective it is useful in trying to understand the effects. We see there is an extremely large difference between the calorically perfect and equilibrium gas values. For flow behind the shock a significant amount of energy goes into dissociation of the gas instead of temperature.

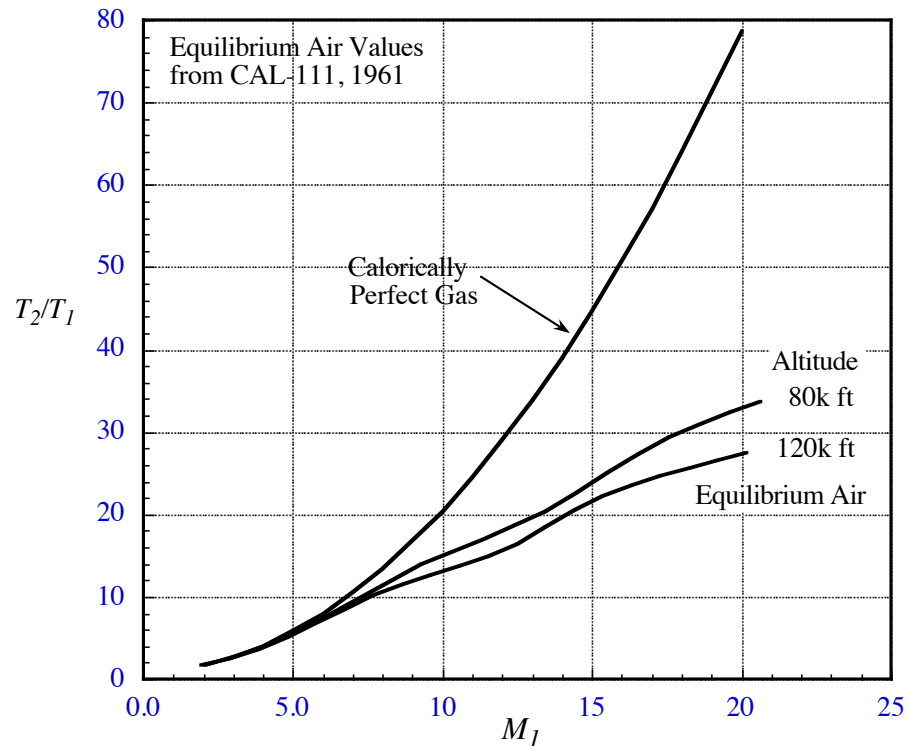


Figure 11-21. Temperature jump across a normal shock wave

According to Anderson,  $\gamma$  is not constant above about 980°F (800°K). Oxygen starts to dissociate above about 3,140°F (2000°K) and is completed at 6,740°F (4000°K). Nitrogen dissociation begins at 15,740°F (9000°K). Above 15,740°F (9000°K), gas starts to ionize and become a plasma. Clearly these are temperatures more closely connected to reentry vehicles than any atmospheric flight vehicles.

We also present the values for the change in pressure and density across the normal shock. The density jump is presented in Figure 11-22 and pressure jump is presented in Figure 11-23. The density is strongly affected by the strong shock. Conversely, the pressure difference between equilibrium air and the calorically perfect gas case is small. Anderson<sup>2</sup> shows that the pressure is more closely connected to the fluid mechanics of the shock jump, while the temperature and density are the result of the thermodynamics of the shock jump.

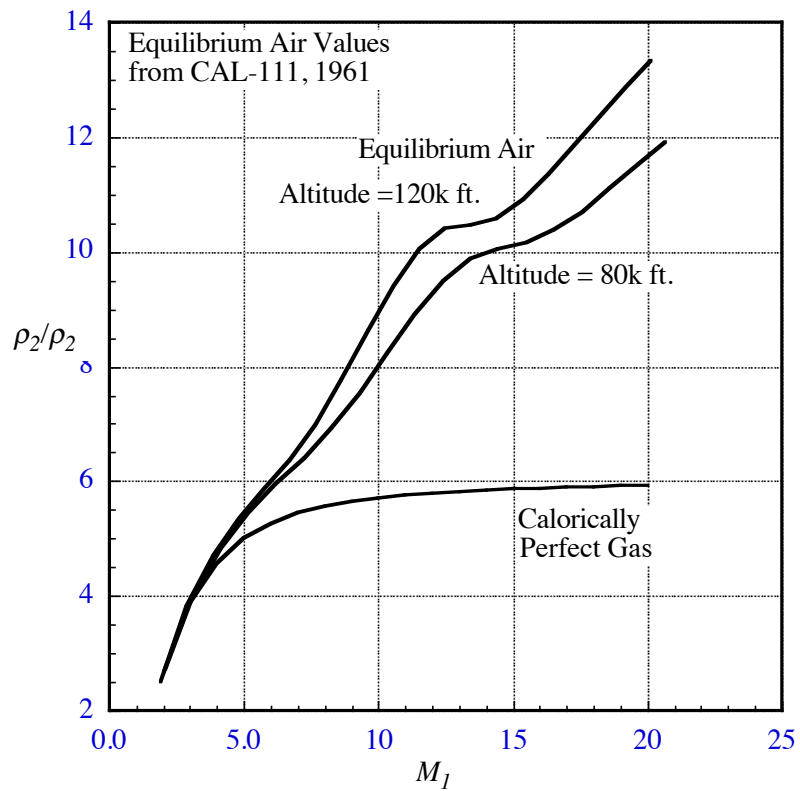


Figure 11-22. Density jump across a normal shock wave.

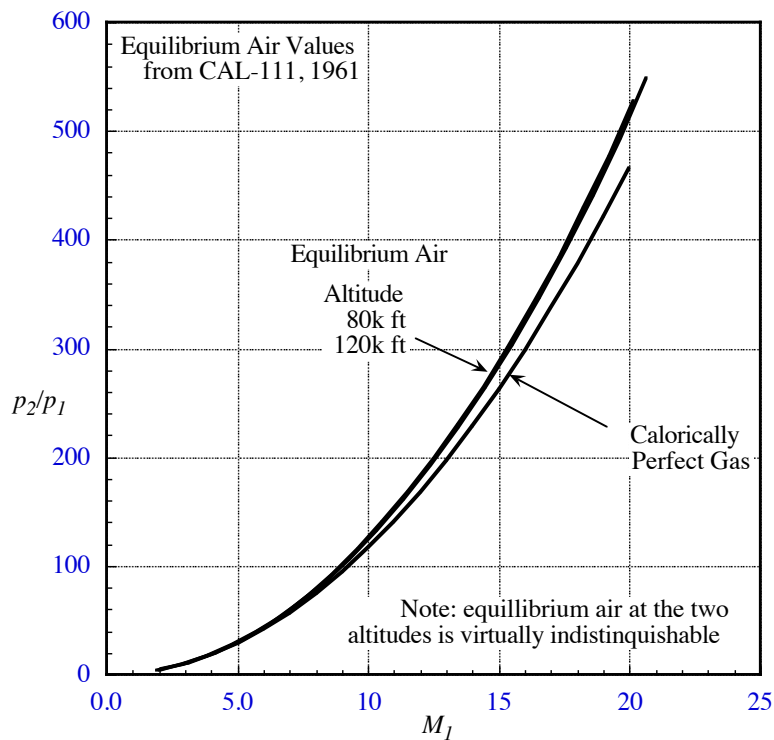


Figure 11-23. Pressure jump across a normal shock wave.

To illustrate the importance of including high temperature effects we describe a situation where the space shuttle was almost lost, apparently because the high temperature gas effects were not included in the predictions, during the first reentry. The difference between the perfect gas and equilibrium air simulation for the pitching moment is shown in Fig. 11-24.<sup>32</sup> There is a significant difference between the predictions. One of the controls on the space shuttle is the “body flap” used to trim the shuttle. It is barely visible in the side view of the shuttle below the rocket nozzle. The flap is shown in more detail in Figure 11-25. It has a limited deflection range. At a Hypersonics Short Course given at the State University of New York at Buffalo on August of 1986 a speaker said that the predicted body flap deflection required to trim had been 11 degrees. It turned out they needed a 16 degree deflection to trim, which was nearly all that was available! The pressure distributions didn’t look very different between the two simulations, but the cumulative effect was extremely important.

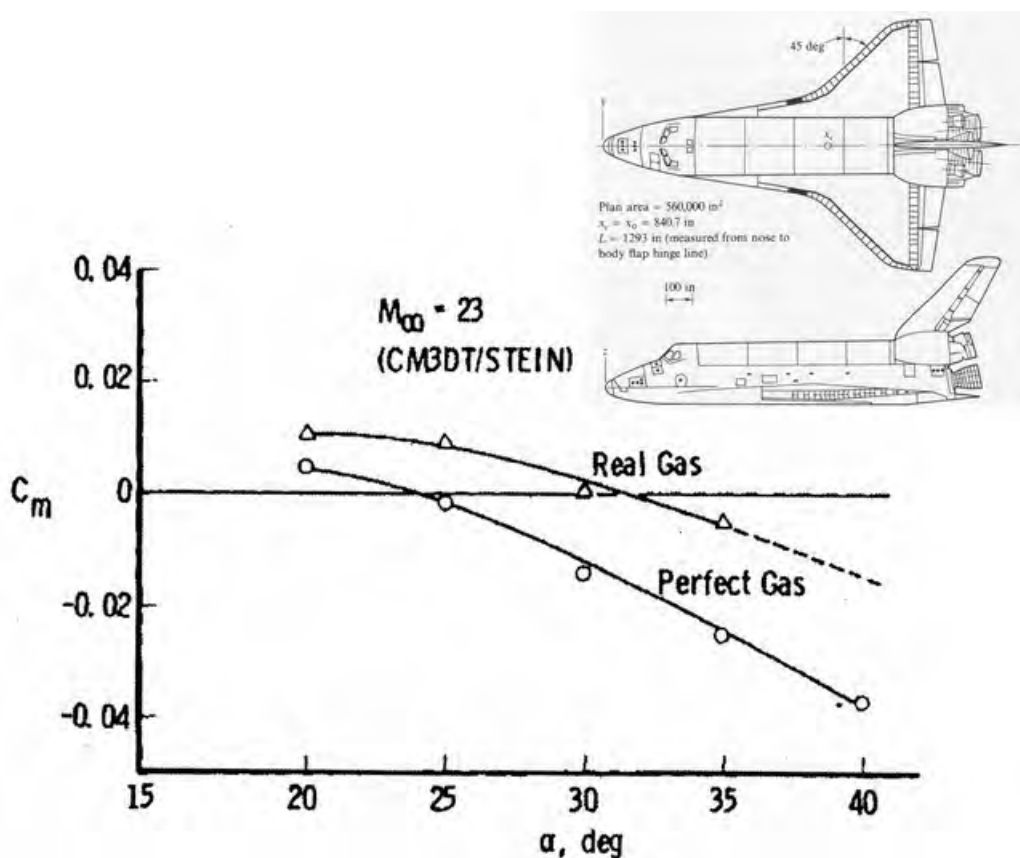


Figure 11-24 Space Shuttle Pitching moment changes with gas model<sup>32</sup>  
(CM3DT and STEIN are the names of the codes used)

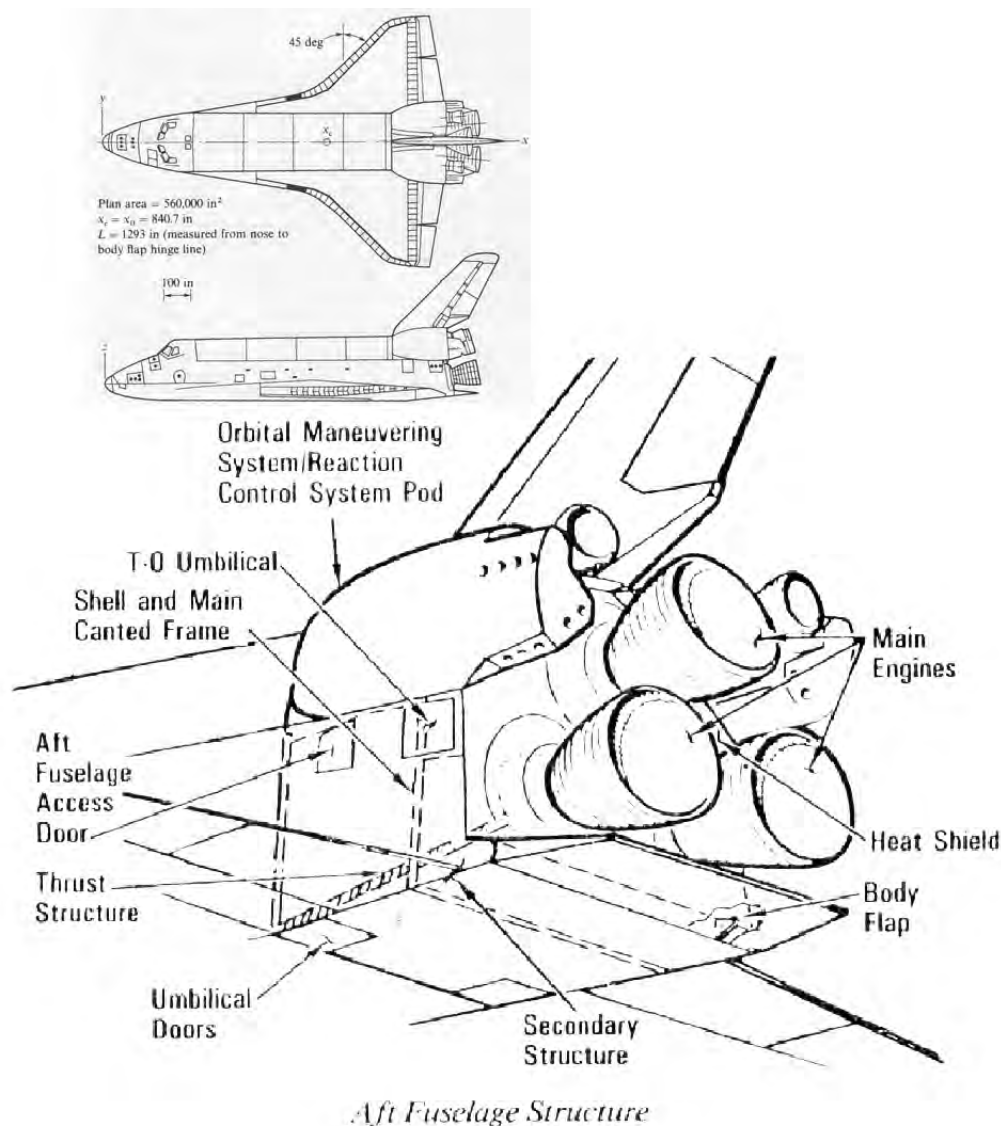


Figure 11-25 Space Shuttle Body flap illustration

Figure 11-26 is a photo of the body flap on the Space Shuttle Discovery, as displayed at the Smithsonian National Air and Space Museum at the Udvar-Hazy Center. Discovery made 39 flights, with the last one on Feb. 24, 2011. It is worth visiting the museum to see Discovery. It is notable that the surface is not at all smooth. This is in contrast to the previous shuttle on display, Enterprise. That shuttle never flew into space and hence never reentered the atmosphere. Its surface is very smooth (Enterprise is currently on display on the Intrepid Sea, Air and Space Museum in the New York City harbor).

Although this explanation of the pitching moment discrepancy seems completely plausible, there have been other explanations. More details of the problem are contained in the discussion by Bertin,<sup>26</sup> see pages 141 – 147. This variety of opinions illustrates the importance of studying problems independently and developing judgment as a configuration aerodynamicist.

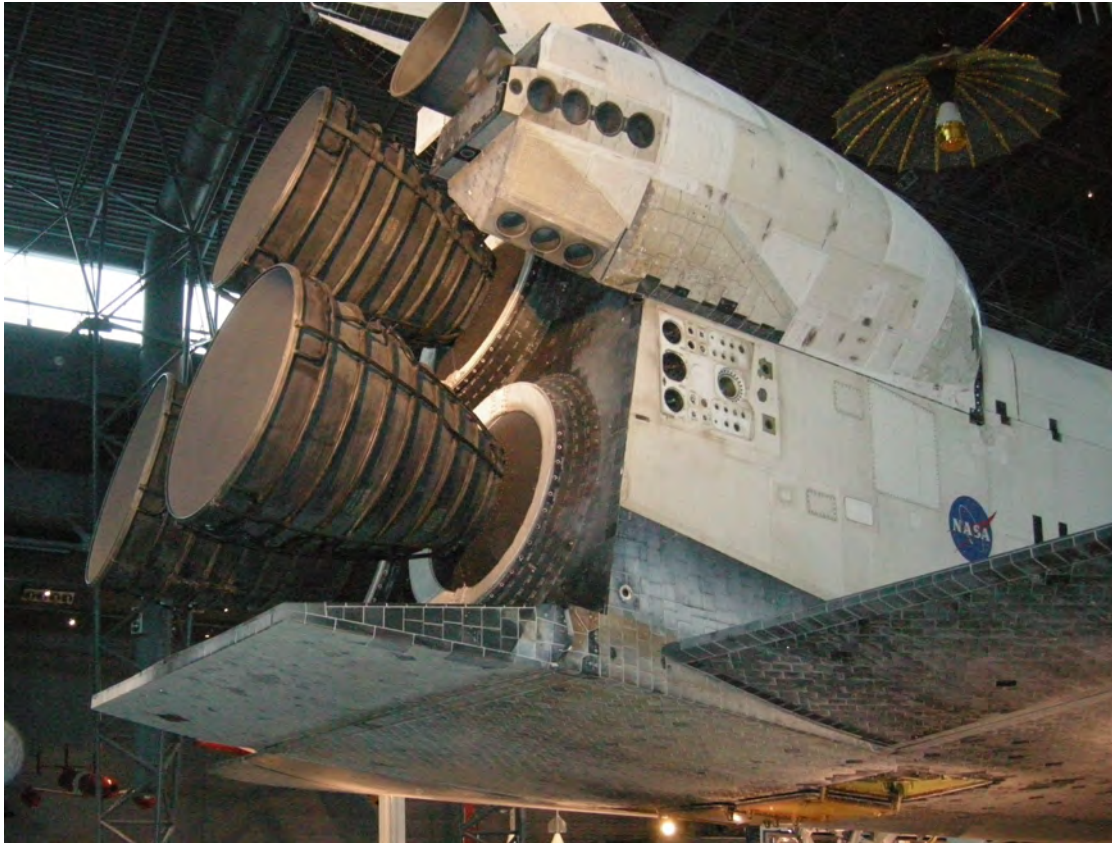


Figure 11-26 Space Shuttle Body Flap photo of the Discovery at the National Air and Space Museum Udvar-Hazy Center

### 11.7 Hypersonic Vehicle Design

Hypersonic flight vehicles encompass a wide variety of applications. Rockets and missiles have become routine. We described the evolution of the shape required to survive the aerodynamic heating environment for entry above, where the use of blunt shapes enabled success. Although hypersonic transports have been the dream of aerodynamicists for many years, we are still a long way from having them. Good histories of hypersonic efforts have been written by Hallion<sup>33</sup> and Heppenheimer<sup>34</sup> (the latter is available as a free pdf file that can be downloaded). As histories, they focus on vehicle efforts as well as the associated technology development.

#### 11.7.1 Minimum drag axisymmetric shapes at hypersonic speeds

Before discussing flight vehicles it is worth reviewing the shapes of minimum drag bodies of revolution at hypersonic speeds. Using the Newtonian pressure formula, Equation 11-2, the minimum forebody drag can be found for a variety of constraints using the calculus of variations. Eggers *et al* did this analysis and presented it together with wind tunnel test verification results.<sup>35</sup> They considered five cases. These were: given (i) forebody length and base diameter, (ii) length and volume, (iii) length and wetted surface area, (iv) diameter and wetted surface area, and (v) diameter and volume. Surprisingly, they found that when the body length is fixed the body has a blunt nose. If the length is not fixed the body has a sharp nose. They also found that when the diameter and wetted surface area are specified the minimum drag forebody shape is a cone.

When the length and diameter are given, the minimum drag forebody shape has “as much as” 20 percent less forebody drag than a cone of the same fineness ratio. Although the theoretical results lead to a “blunt” nose, the radius at the nose is actually very small. Furthermore, the forebody shape is very closely approximated by the power law shape:

$$\frac{r}{r_{base}} = \left(\frac{x}{l}\right)^n \quad (11-19)$$

where the value of  $n$  is 0.75 for the minimum drag body of given length and diameter. Many other variations of minimum drag bodies have been found and collected in a book edited by Angelo Miele.<sup>36</sup>

Because of the interest in minimum drag shapes, work has been done using CFD to verify the results found from Newtonian Theory.<sup>37</sup> A power law body was studied with various values of  $n$ . The CFD results found the minimum drag exponent to be very nearly an  $n$  of 0.69, and the drag was indeed about 20% less than a cone with the same length and diameter. The result of the computational study is shown in Figure 11-27.

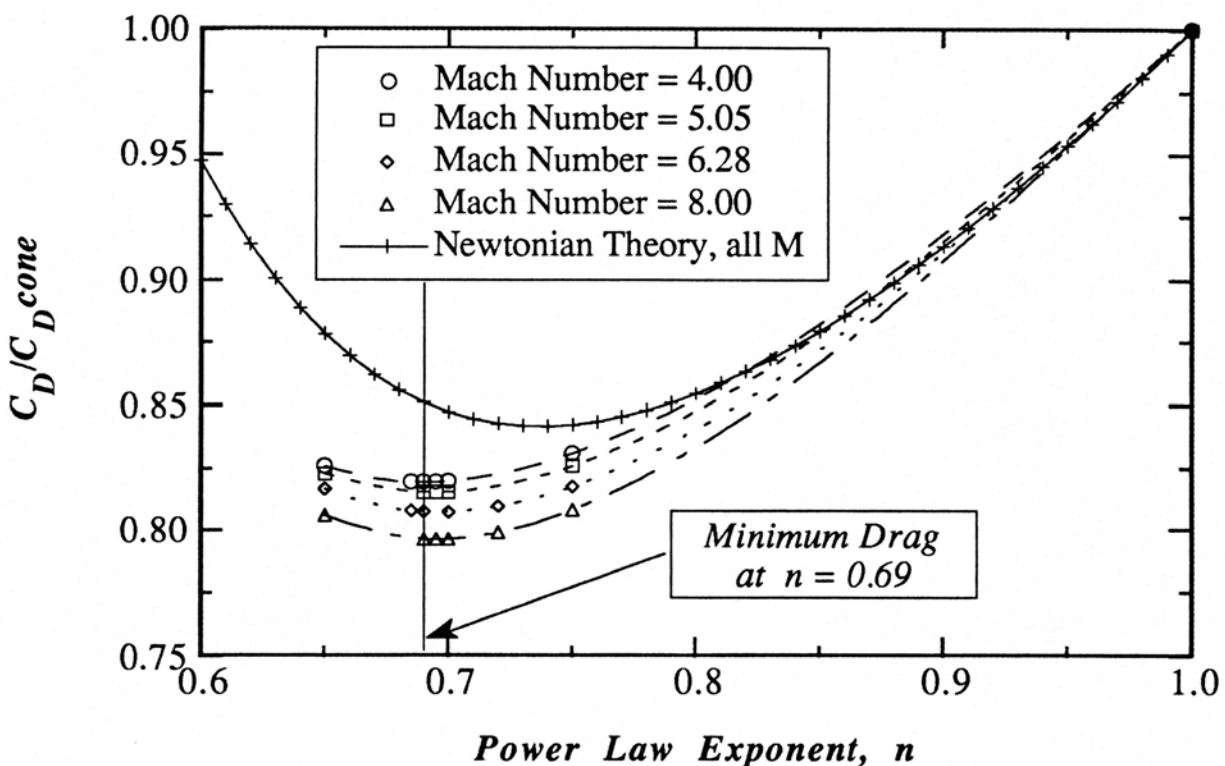


Figure 11-27. Numerical determination of the optimum “ $n$ ” for power law shapes.<sup>37</sup>

Note that power law bodies with an  $n$  greater than 0.50 have a peculiar property. The slope at the nose is  $90^\circ$ , but there is no longer a leading edge radius. So the shape could be described as “blunt”, but only weakly!<sup>38</sup>

### 11.7.2 Brief review of hypersonic flight vehicles

A description of “recent” efforts should probably start with NASP. This was the acronym for the National Aero-Space Plane concept, although considerable work had been done previously.<sup>39,40,41</sup>

Based on hopes and dreams, this program was announced publicly by President Ronald Reagan in his 1986 State of the Union address. It was to be a single-stage to-orbit (SSTO) vehicle and a passenger plane capable of a two-hour flight from Washington to Tokyo. Anyone who has taken a propulsion course and studied the staging equations understands the difficulty of developing a successful SSTO. Nevertheless, a large government program was started. The first step was to be the X-30 demonstrator. An artist's conception of the plane is given in Figure 11-28. Recall that rockets have to carry both the oxidizer and the fuel. It was hoped that the X-30 would be viable because it would employ a propulsion system that used atmospheric air for most of the oxidizer. This would result in a large weight savings. The propulsion system envisioned is known as a scramjet (remember the X-15 fiasco described above when they carried a dummy scramjet engine). This is a ramjet where the incoming flow is only slowed to supersonic speed in the combustor. A book is now available to provide details of scramjet propulsion systems.<sup>42</sup> When the NASP program was initiated no scramjet had been demonstrated! The development of such a system is still ongoing, clearly very slowly. The NASP program was cancelled in 1993.

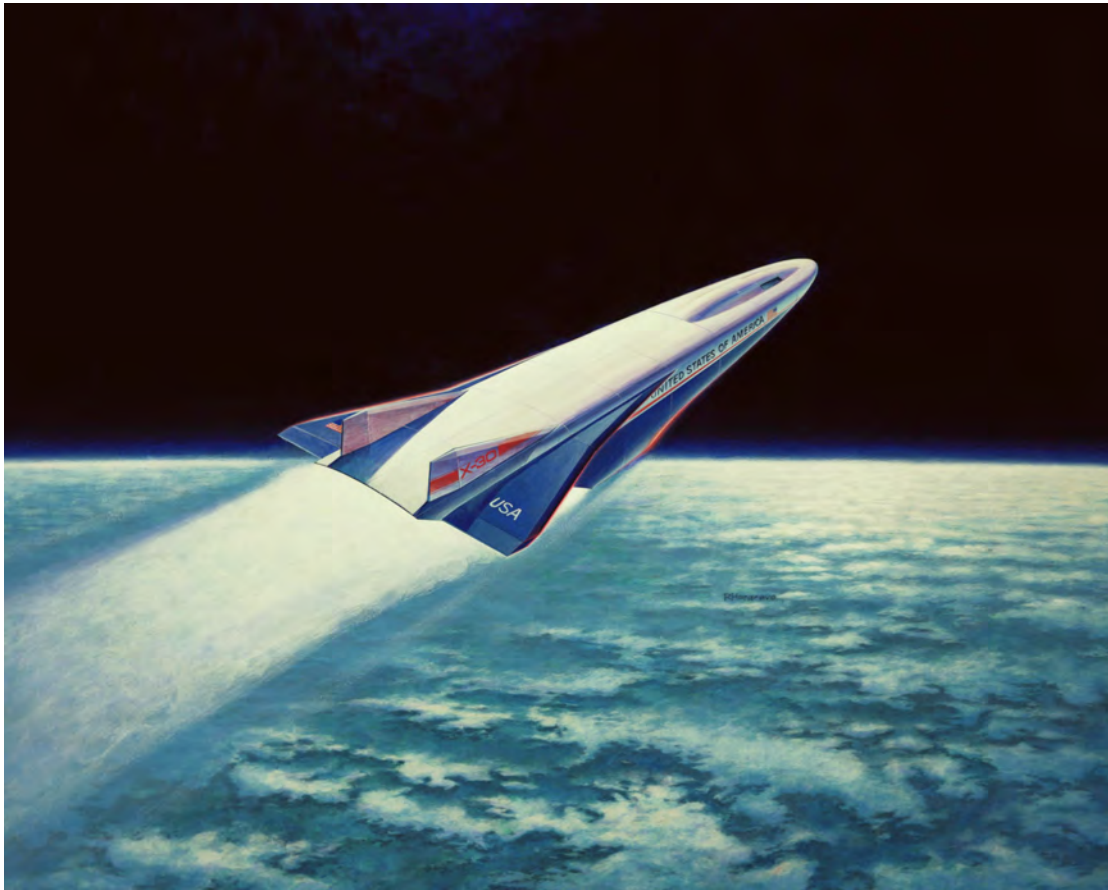


Figure 11-28. The NASP Concept (downloaded from a Google image search)

### 11.7.3. Engine-airframe Integration and Modern Vehicle Development

More recent efforts have been much more modest. Clearly the first step had to be a successful demonstration of a scramjet propulsion system. This requires flight demonstration because no ground-based facilities have the capability to simulate the flight environment. This requirement led to a concept known as Hyper-X, that became the X-43. A description of the evolution of this concept is described in a highly readable book by Curtis Peebles.<sup>43</sup> As we saw above in Figure

11-5, all of the important forces are on the lower surface of a hypersonic vehicle. Therefore, it had become clear that the airframe and engine would rely on controlling the lower surface flowfield. In effect the forebody became the inlet and the aft body became the nozzle. Figure 11-29 illustrates the concept.

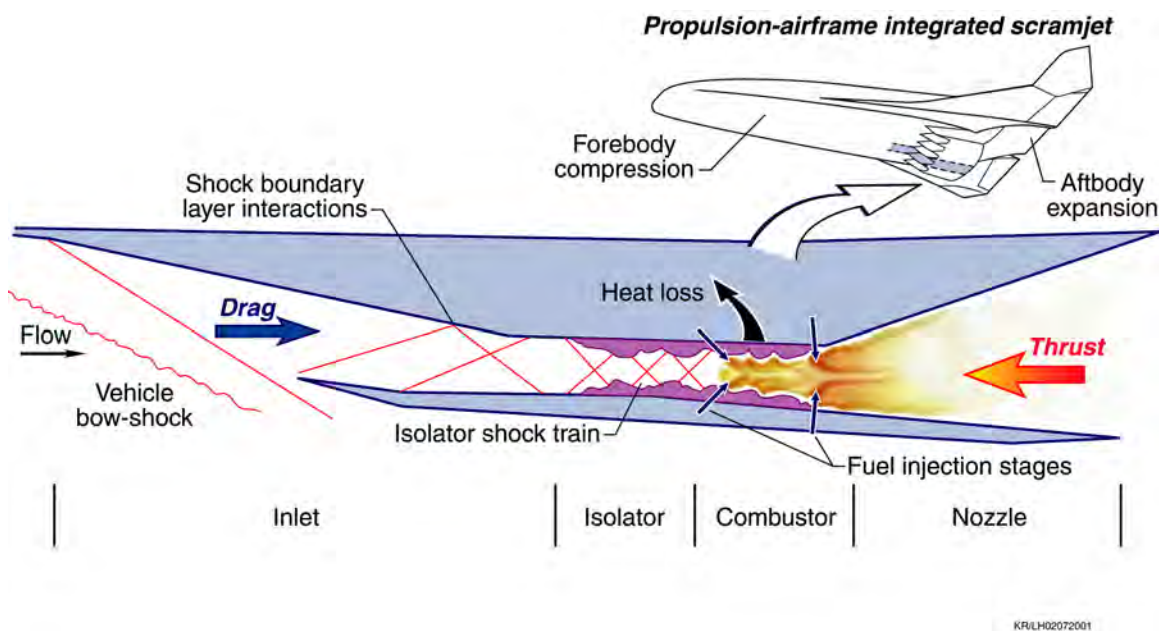


Figure 11-29. Example of engine-airframe integration for a hypersonic aircraft (from Walt Engelund, NASA Langley, May 2001).

The X-43 was mounted on the Orbital Sciences Pegasus vehicle, that was rocket powered, dropped from a B-52. It boosted the X-43 to the speed where it could be separated from Pegasus and scramjet powered propulsive flight. The first attempt resulted in a Pegasus failure on June 2, 2001. Subsequently there were two successful flights of the X-43. The second flight occurred on March 27, 2004 and achieved a Mach number of 6.83 after 10 seconds of powered flight (the  $q$  was 980psf at 110k ft altitude). The 3<sup>rd</sup> flight on Nov. 16, 2004 reached a Mach number of 9.68 with 11 seconds of powered flight (also at 110K ft. altitude). Note that the vehicles came down in the Pacific Ocean and were never recovered. All the results were obtained from onboard telemetry. Figure 11-30 provides an idea of what the X-43 actually looked like.

The November-December 2001 issue of the *Journal of Spacecraft and Rockets* had a special section devoted to the Hyper-X and in 2006 the AIAA Dryden Lectureship was given on the X-43.<sup>44</sup> That paper shows that a surface temperature as high as 2000°F was measured.



Figure 11-30 Artist conception of the X-43 in flight

The next step in the evolution of hypersonic air-breathing vehicles is the X-51. This is known as a “Wave Rider” concept. Waveriders provide efficient hypersonic flight. The designs can be thought of as placing a shape in the streamline of a body-generated flowfield so that the bottom surface is “resting” on the pressure field generated by the shock wave of this flowfield. The arrangement is designed to obtain lift with very low drag. See Bertin and Cummings<sup>1</sup> for a good, detailed description of waveriders. At one time waveriders had a precise definition, but currently it appears to refer to any concept that exploits lower surface lift. The application of the X-51 type vehicle is likely a missile. The X-51 concept is shown in Figure 11-31. It is 25 feet long and weighs 4,000 lb.

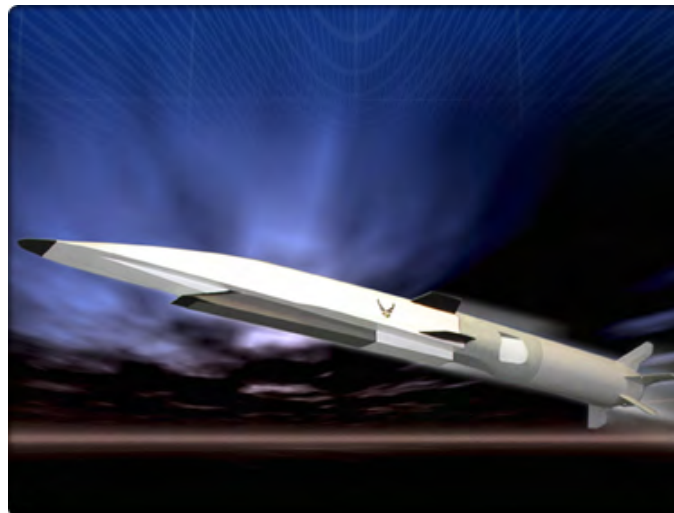


Figure 11-31 The X-51 Waverider (provided by Karen Berger of NASA Langley).

The first flight of the X-51 took place on May 26, 2010, and achieved 200 seconds of powered flight, reaching a speed of Mach 5 at 70,000 feet. The 2<sup>nd</sup> flight had a problem when the scramjet

had an “unstart” when they tried to switch from ethylene to JP-7 as fuel. On the 3<sup>rd</sup> flight a control fin locked up and the vehicle went out of control. On the fourth flight, May 1, 2013, they had success with 210 seconds of flight at a Mach number of 5.21.

Clearly significant progress was made between the X-43 and X-51. This also illustrates the importance of maturing a technology before undertaking a vehicle development program. Any air-breathing hypersonic vehicle will have a highly integrated engine and airframe. To reiterate, in these concepts the hypersonic propulsion will be provided by a scramjet engine, which obtains thrust with a combustion chamber in which the flow is supersonic. Figure 11-29, from a presentation to the class by Walt Engelund of NASA Langley, showed this. The entire forebody of the vehicle underside is used as an external inlet to provide flow at just the right conditions to the engine. The entire underside afterbody is the exhaust nozzle. The successful design of an airbreathing hypersonic vehicle is an excellent example of the need for multidisciplinary optimization methods. This is a very hard problem and the structure, aero-dynamics and propulsion system are very tightly integrated. Two reviews are available with more details.<sup>45,46</sup>

With the recent progress with scramjet vehicles we can expect to see designs proposed using this technology. However, remember that the vehicle must still be boosted to a high enough Mach number for the scramjet propulsion system to start. It will be interesting to see how these concepts are developed in the future.

### 11.8 Exercises

1. Derive expressions for the lift curve slope of a flat plate and a wedge using linear supersonic theory and Newtonian theory. Comment on the differences and implications for aircraft design.
2. Derive the expression for  $C_{p_{max}}$  used in the modified Newtonian theory formula. Show that with  $\gamma = 1.4$ , the value for  $M = \infty$  is 1.84, and at  $M = 4$ ,  $C_{p_{max}}$  is 1.79.
3. Using the estimate given below for the adiabatic wall temperature, what is the surface temperature at Mach 2 for an airplane flying at 60,000 ft altitude? What is it if the airplane is flying at  $M = 3$ ?

$$T_{AW} = \left( 1 + r \frac{\gamma - 1}{2} M_{\infty}^2 \right) T_e$$

where  $r = 0.85$  for laminar flow and 0.88 for turbulent flow.

What is your conclusion? (This should be less than one page of analysis.)

4. Consider a wedge with a half angle of  $\theta$ . Find  $C_{L\alpha}$  assuming both linear supersonic theory and hypersonic Newtonian theory for the pressure coefficients. How does the lift curve slope vary with  $\theta$  and Mach number for the two different flow models? What are the configuration implications?
5. Read Ben Rich's Paper

Ben R. Rich, “F-12 Series Aircraft Aerodynamic and Thermodynamic Design in Retrospect,” *Journal of Aircraft*, Vol.11, No. 7, July 1974, pp. 401-406.

Turn in the usual 1-page summary of what you learned.

## 11.9 References

---

- <sup>1</sup> John J. Bertin and Russell M. Cummings, *Aerodynamics for Engineers*, Pearson Prentice Hall, Upper Saddle Brook, 2009.
- <sup>2</sup> John Anderson, *Hypersonic and High Temperature Gas Dynamics*, McGraw-Hill, New York, 1989 (now published by the AIAA).
- <sup>3</sup> Milton O. Thompson, *At the Edge of Space: The X-15 Flight Program*, Smithsonian Institution Press, Washington, 1992.
- <sup>4</sup> Charlie M. Jackson, Jr., and Wallace C. Sawyer, "A Method for Determining Surface Pressures on Blunt Bodies of Revolution at Small Angles of Attack in Supersonic Flow," NASA TN D-4865, 1968 Note this report includes results from a wind tunnel test, and has the tab data.
- <sup>5</sup> Fred R. DeJarnette, C.P. Ford and D.E. Young, "A New Method for Calculating Surface Pressures on Bodies at an Angle of Attack in Supersonic Flow," AIAA 1979-1552, July 1979.
- <sup>6</sup> Sims, J. L., "Tables for Supersonic Flow Around Right Circular Cones at Zero Angle of Attack," NASA SP-3004, 1964.
- <sup>7</sup> Public Domain Aeronautical Software, <http://www.pdas.com>
- <sup>8</sup> Charles McLellan, "A Method for Increasing the Effectiveness of Stabilizing Surfaces at High Supersonic Mach Numbers," NACA RM L54F21, Aug. 1954, Declassified: 1958.
- <sup>9</sup> Roxanah B. Yancy, "Flight Measurements of Stability and Control Derivatives of the X-15 Research Airplane to a Mach Number of 6.02 and an Angle of Attack of 25°." NASA TN D-2532, 1964.
- <sup>10</sup> Bob Hoey, "X-15 Ventral Off," in *Flight Testing at Edwards, Flight Test Engineers' Stories 1946 – 1975*, edited by Fred Stoliker, Bob Hoey and Johnny Armstrong, Flight Test Historical Foundation, 1996.
- <sup>11</sup> John J. Bertin and Russell M. Cummings, "Fifty years of hypersonics: where we've been, where we're going", *Progress in Aerospace Sciences*, Vol. 39, pp. 511-536, 2003 (Note: ignore the error in the first line of the abstract that has the wrong date and pilot for the Mach 6.7 flight)
- <sup>12</sup> Ben R. Rich, "F-12 Series Aircraft Aerodynamic and Thermodynamic Design in Retrospect," *Journal of Aircraft*, Vol.11, No. 7, July 1974, pp. 401-406.
- <sup>13</sup> H. Julian Allen and A.J. Eggers, Jr., "A Study of the Motion and Aerodynamic Heating of Ballistic Missiles Entering the Earth's Atmosphere at High Supersonic Speeds," NACA Report 1381, 1958 (date when the work was declassified).
- <sup>14</sup> Milton Van Dyke, assembler, *An Album of Fluid Motion*, Parabolic Press, 1982.
- <sup>15</sup> James E. Pavlosky and Leslie G. St. Leger, "Apollo Experience Report – Thermal Protection Subsystem," NASA TN D-7564, 1974.
- <sup>16</sup> Gino Moretti and Mike Abbett, "A Time Dependent Computational Method for Blunt Body Flows," *AIAA Journal*, Vol. 4, No. 12, 1966, pp. 2136-2141.
- <sup>17</sup> Kenneth W. Iliff and Mary F. Shafer, "A Comparison of Hypersonic Flight and Prediction Results," AIAA Paper 93-0311, Jan. 1993.

- <sup>18</sup> Joe D. Watts, "Flight Experience with Shock Impingement and Interference Heating on the X-15-2 Research Airplane," NASA TM X-1669, 1968.
- <sup>19</sup> Wallace D. Hayes and Ronald F. Probstein, *Hypersonic Flow Theory*, Academic Press, New York, 1959.
- <sup>20</sup> Mitchel H. Bertram, "An Approximate Method for Determining the Displacement Effects and Viscous Drag of Laminar Boundary Layers in Two-Dimensional Hypersonic Flow," NACA 2773, 1952.
- <sup>21</sup> FRICTION, [http://www.dept.aoe.vt.edu/%7Emason/Mason\\_f/MRsoft.html](http://www.dept.aoe.vt.edu/%7Emason/Mason_f/MRsoft.html)
- <sup>22</sup> F.M. White in *Viscous Fluid Flow*, McGraw-Hill, New York, 1974, pp. 589-590.
- <sup>23</sup> E.J. Hopkins, "Charts for Predicting Turbulent Skin Friction from the Van Driest Method (II)," NASA TN D-6945, October 1972.
- <sup>24</sup> Russell M. Cummings, "Numerical Simulation of Hypersonic Flows," *Journal of Spacecraft and Rockets*, Vol. 52, No. 1, Jan-Feb. 2015, pp. 15-16. This is an overview of the papers contained in this special section.
- <sup>25</sup> Chris Johnston, NASA Langley Research Center, personal communication.
- <sup>26</sup> John J. Bertin, *Hypersonic Aerothermodynamics*, AIAA, Washington, 1994.
- <sup>27</sup> Ernst Heinrich Hirschel and Claus Weiland, *Selected Aerothermodynamic Design Problems of Hypersonic Flight Vehicles*, Springer, Berlin, 2009.
- <sup>28</sup> Brian R. Hollis and Salvatore Borrelli, "Aerothermodynamics of Blunt Body Entry Vehicles," *Progress in Aerospace Sciences*, Vol. 48-49, Jan-Feb 2012, pp. 42-56.
- <sup>29</sup> Charles E. Wittliff and James T. Curtis, "Normal Shock Wave Parameters in Equilibrium Air," CAL Report No. CAL-111, Nov. 1961.
- <sup>30</sup> <http://www.engapplets.vt.edu>
- <sup>31</sup> Srinivasan S, Tannehill J C and Weilmuenster K J. "Simplified Curve Fits for the Thermodynamic Properties of Equilibrium Air", NASA RP 1181, August 1987.
- <sup>32</sup> J. R. Maus, B. J. Griffith, K.Y. Szema and J.T. Best, "Hypersonic Mach Number and Real Gas Effects on Space Shuttle Orbiter Aerodynamics," *Journal of Spacecraft and Rockets*, Vol. 21, No. 2, March-April 1984, pp. 136-141.
- <sup>33</sup> Richard P. Hallion, "The History of Hypersonic: or, "Back to the Future – Again and Again", AIAA Paper 2005-0329, 2005.
- <sup>34</sup> T. A. Heppenheimer, *Facing the Heat Barrier: A History of Hypersonics*, NASA SP-2007-4232, 2007.
- <sup>35</sup> A.J. Eggers, Jr., Meyer M. Resnikoff and David H. Dennis, "Bodies of Revolution Having Minimum Drag at High Supersonic Airspeeds," NACA R 1306, 1958.
- <sup>36</sup> Angelo Miele, editor, *Theory of Optimum Aerodynamic Shapes*, Academic Press, New York, 1965.
- <sup>37</sup> W. H. Mason and Jaewoo Lee, "Minimum-Drag Axisymmetric Bodies in the Supersonic/Hypersonic Flow Regime," *Journal of Spacecraft and Rockets*, Vol. 31, No. 3, May-June 1994, pp. 406-412.
- <sup>38</sup> W. H. Mason and Jaewoo Lee, "Aerodynamically Blunt and Sharp Bodies," *Journal of Spacecraft and Rockets*, Vol. 31, No 3, May-June 1994, pp. 378-382.

- 
- <sup>39</sup> Thomas J. Gregory, Richard H. Petersen and John A. Wyss, "Performance Tradeoffs and Research Problems for Hypersonic Transports," *Journal of Aircraft*, Vol. 2, No. 4, July-Aug 1965, pp. 266-271.
- <sup>40</sup> Richard H. Petersen, Thomas J. Gregory and Cynthia L. Smith, "Some Comparisons of Turboramjet-Powered Hypersonic Aircraft for Cruise and Boost Missions," *Journal of Aircraft*, Vol. 3, No. 5, Sept.-Oct. 1966, pp. 398-405.
- <sup>41</sup> David A. Fetterman, Charles H. McLellan, L. Robert Jackson, Beverly Z. Henry, Jr., and John R. Henry, "A Review of Hypersonic Cruise Vehicles," NASA TM X-1276, 1966.
- <sup>42</sup> Corin Segal, *The Scramjet Engine – Processes and Characteristics*, Cambridge Univ. Press, New York, 2009.
- <sup>43</sup> Curtis Peebles, *Road to Mach 10 – Lessons Learned from the X-43A Flight Research Program*, AIAA, Reston, 2008. (the book includes a DVD with videos and a collection of AIAA and NASA Reports)
- <sup>44</sup> Charles R. McClinton, "X-43 – Scramjet Power Breaks the Hypersonic Barrier, Dryden Lectureship in Research for 2006," AIAA Paper 2006-1, Jan. 2006.
- <sup>45</sup> Mary Kae Lockwood, Dennis Petley, John G. Martin and James L. Hunt, "Airbreathing hypersonic vehicle design and analysis methods and interactions," *Progress in Aerospace Sciences*, Vol. 35, pp 1-32, 1999.
- <sup>46</sup> Kevin G. Bowcutt, "Multidisciplinary Optimization of Airbreathing Hypersonic Vehicles," *Journal of Propulsion and Power*, Vol. 17, No. 6, Nov-Dec 2001, pp 1184-1190.